Order Number 1349473

Improved thermometry system for ultrasound hyperthermia

Lim, Chuck Mang, M.S.

The University of Arizona, 1992

U·M·I
300 N. Zeeb Rd.
Ann Arbor, MI 48106

IMPROVED THERMOMETRY

SYSTEM FOR ULTRASOUND HYPERTHERMIA

by

Chuck Mang Lim

A Thesis Submitted to the Faculty of the

DEPARTMENT OF ELECTRICAL AND COMPUTER ENGINEERING

In Partial Fulfillment of the Requirements
For the Degree of

MASTER OF SCIENCE
WITH A MAJOR IN ELECTRICAL ENGINEERING

In the Graduate Collage

THE UNIVERSITY OF ARIZONA

1992

STATEMENT BY AUTHOR

This thesis has been submitted in partial fulfillment of requirements for an advanced degree at The University of Arizona and is deposited in the University Library to be made available to borrowers under rules of the Library.

Brief quotations from this thesis are allowable without special permission, provided that accurate acknowledgment of source is made. Requests for permission for extended quotation from or reproduction of this manuscript in whole or in part may be granted by the head of the major department or the Dean of the Graduate College when in his or her judgment the proposed use of the material is in the interests of scholarship. In all other instances, however, permission must be obtained from the author.

SIGNED: Sam Chuck Mang

APPROVAL BY THESIS DIRECTOR

This thesis has been approved on the date shown below:

Hal S. Tharp — 7/24/92

Hal S. Tharp
Assistant Professor of
Electrical and Computer Engineering

Date

ACKNOWLEDGMENTS

The author would like to express sincere thanks to Dr. R.B. Roemer, Dr. K. Hynynen, Dr. H.S. Tharp and Dr. A.F. Witulski for their constant advice, guidance and encouragement during the research process. Special thanks go to Dennis Anhalt, Scott Nathanson, Mark Buchanan, Eugene Gross, Andrew Dutton and Matt Rademacher who provided friendship, technical support and advice for the duration of this work.

The author would like to give greatest thanks to his family, especially to his parents, Aik Hai Lim and Kwang Lang Ang; although far away, they always provided love and moral support in this project and many that came before.

This research has been supported by NCI grant 33922.

TABLE OF CONTENTS

LIST OF FIGURES 7

LIST OF TABLES 8

ABSTRACT 9

1. INTRODUCTION 10
1.1 Introduction to ultrasound hyperthermia 10
1.2 Background of ultrasound hyperthermia thermometry system 12
1.2.1 Thermocouple theory 12
1.2.2 Artifact 16
1.2.3 Isolation 18
1.2.4 Speed of temperature acquisition 20
1.3 Previous thermometry system at UACC 21
1.4 Improved thermometry system 22

2. HARDWARE DESCRIPTION 23
2.1 System hardware setup 23
2.2 Bus driver buffer 24
2.3 Temperature Acquisition Unit 26
2.3.1 Amplifier card 26
2.3.1.1 Functional description of amplifier and A/D converter 28
2.3.1.2 Reference junction measurement 33
2.3.2 Card select and pulsing card 37
2.4 Opto-isolation unit 42
2.5 Hardware performance 44
2.5.1 Speed of temperature acquisition 44
2.5.2 Isolation performance 45
2.5.2.1 Isolation measurement 45

3. TWO POINT CALIBRATION AND REFERENCE JUNCTION COMPENSATION 47
3.1 Calibration technique 47
3.1.1 Two point calibration 49
3.1.2 Reference junction compensation 51
3.1.3 Equipment temperature compensation 52
3.1.4 Calibration equation 59
3.1.5 Data storage format 64

TABLE OF CONTENTS - *continued*

3.2 Temperature read flow chart 66
3.3 Calibration results and accuracy 66

4. SENSOR LOCATING SYSTEM 70
4.1 Hardware set up for sensor locating routine 72
4.2 Search strategy 75
4.3 Locate operation 77
4.4 Search path 79
4.5 Flow chart of locate routine 81
4.6 Experimental results of locate routine 81
4.7 Comparison of multi-sensor vs. single sensor search 86
4.8 Problems in the multi-sensor search 88
4.8.1 Out of boundary 89
4.8.2 The diameter of the focus 90
4.8.3 Depth of the focus 91
4.8.4 Search resolution 92
4.8.5 Reflections 93
4.9 Noise rejection 93

5. DISCUSSION, CONCLUSIONS AND SUGGESTIONS FOR FUTURE WORK 96

APPENDIX A: THERMOMETRY SYSTEM I SCHEMATIC 101
APPENDIX A.1 Bus driver buffer schematic 102
APPENDIX A.2 Opto-isolation unit schematic 103
APPENDIX A.3 Card select and pulsing card schematic 104
APPENDIX A.4 Amplifier card schematic 105

APPENDIX B: THERMISTOR DATA 106

APPENDIX C: VERSION 2 TAU 107
C.1 General modification 108
C.1.1 General structural modification 108
C.1.2 Amplifier layout modification 108
C.2 Electrical hardware modification 110
C.2.1 Buffer card modification 110
C.2.2 Opto-isolation card modification 111
C.2.3 Amplifier card modification 112

TABLE OF CONTENTS - *continued*

APPENDIX D: CONNECTORS 115

APPENDIX E: SYSTEM SOFTWARE 117

REFERENCES 118

LIST OF FIGURES

Figure 1.1 Thermocouple circuit of metal A and B 13
Figure 1.2 Thermocouple voltage measurement 14
Figure 1.3 Reference junction compensation 15
Figure 1.4 Equivalent reference junction arrangement 16
Figure 1.5 Simplified patient electrical safety with medical equipment 18
Figure 2.1 Thermometry System block diagram 25
Figure 2.2 TAU block diagram 27
Figure 2.3 Amplifier card block diagram 29
Figure 2.4 Constant current source circuit 34
Figure 2.5 Card select and pulsing card block diagram 38
Figure 2.6 TAU timing diagram 41
Figure 2.7 Hand shaking signal S to PC 42
Figure 2.8 Opto-isolation unit block diagram 43
Figure 3.1 One and two point calibration offset adjustment 50
Figure 3.2 TAU enclosure top view 53
Figure 3.3 Temperature difference across connector 54
Figure 3.4 Flow chart of temperature read for probes 67
Figure 4.1 System interface to TAU 73
Figure 4.2 Timing diagram of locate temperature read 78
Figure 4.3 Search path 80
Figure 4.4 Flow chart of locate routine 82
Figure 4.5 Ultrasound intensity plot of transducer 83
Figure 4.6 Setup for locate experiment 84
Figure 4.7 Multi-sensor search and single sensor search 87
Figure 4.8 Single sensor search overlap 88
Figure 4.9 Out of boundary search 89
Figure 4.10 Large focus diameter transducer 90
Figure 4.11 Out of focus depth 91
Figure 4.12 Large search resolution 92
Figure 4.13 Reflective material (flat) 94
Figure 4.14 Reflective material (curved) 95
Figure C.1 Version 2 TAU block diagram 109
Figure C.2 Connector position on amplifier card 110
Figure C.3 Buffer card block diagram 111
Figure C.4 Opto-isolation unit block diagram 113
Figure C.5 Amplifier card block diagram 114
Figure D.1 Difference in connector 115

LIST OF TABLES

Table 2.1 TAU memory map 31
Table 2.2 12-bit A/D data storage 40
Table 3.1 Summary of component temperature coefficients 52
Table 3.2 Measured temperatures for determining the temperature coefficient of the amplifiers 56
Table 3.3 Measured temperatures for approximation of temperature coefficient in connector pin difference temperature 57
Table 3.4 Temperature measurement result 68
Table 4.1 Motor pulses (x,y,z,r,t) 74
Table 4.2 Wavetek command codes 75
Table 4.3 Locating system accuracy (mm) data for 10 repeated searches 85
Table B Thermistor current and coefficient 106

ABSTRACT

A thermometry system for use during ultrasound hyperthermia treatments was developed to provide fast and reliable temperature measurements such that transient temperatures from multi-sensor thermocouples could be measured. It was also intended to provide electrical isolation for patient safety when bare thermocouple sensors were used in order to reduce artifacts. The system hardware development involved fabrication of a high precision temperature measurement box which was electrically isolated from, by an opto-isolation unit, and interfaced with, an 386-20 MHz personal computer. The system software development involved a two point calibration program for each thermocouple probe to be used with the system, and a sensor locating program to rapidly identify the probe locations immediately prior to treatment. A single scan temperature reading speed of 0.2 s for all 112 thermocouple sensors with an average accuracy of ± 0.05 °C under normal operating conditions (ambient temperature 22 °C to 28 °C) was achieved. A probe to earth ground leakage sink current of 75 μA and a leakage source current of less than 10 μA was attained.

CHAPTER 1

INTRODUCTION

1.1 Introduction to ultrasound hyperthermia

Scanned focussed ultrasound (SFUS) has been used as a method for hyperthermia therapy for cancer treatments since 1975 [1]. This modality of therapy has also been used at the University of Arizona Cancer Center (UACC) to treat cancer patients with potentially optimistic promising results [11, 25, 26, 27]. The theoretical and practical aspects of focussing ultrasonic waves into tissue which results in a temperature increase are given in detail by Hynynen [2]. The biological damage to tissue due to increased temperature was found to depend on temperature and time [24]. For example, brain is damaged at 42.5 °C when given at least 10^3 s of sonication [23]. If temperatures are higher than 42.5 °C, less time is required for equivalent damage since the relation of time vs. temperature is approximately given as 0.1778 log(s)/°C [24]. With this in mind, it is clear that accurate and reliable thermometry systems must be used during ultrasound hyperthermia.

Thermocouples are the temperature sensors of choice for ultrasound hyperthermia therapy at the UACC. They are relatively inexpensive and easy to manufacture and can be made into very small multi-sensor arrays (seven sensors per

probe in this case). Tissue temperatures during ultrasound hyperthermia are detected by thermocouple sensors which are inserted into the tissue prior to administering the treatment. Thermocouples used at the UACC are encased in polyethylene tubing which provides electrical insulation for patient safety [25]. However, artifact (artificial temperature effect) is introduced during temperature measurement due to the polyethylene tubing [5]. Thus, it is important to remove the polyethylene tubing, if possible, to obtain better temperature information as measured by the thermocouple sensors.

Although temperature reading speed is not a major problem for temperature measurements during SFUS treatments, where the temperature is read at every 30 s interval, it is necessary to have a high speed thermometry system to measure transient temperatures during the location search for sensors and during animal experiments. During SFUS treatments, it is necessary to locate the actual position of the target tumor and surrounding tissues relative to the ultrasound transducer focal point. The thermocouple locations are identified by the maximum rate of temperature rise of the thermocouple sensors relative to the transducer position [12]. Thus, transient temperatures are read during the location search. Therefore a high speed thermometry system will provide efficient transient temperature measurement during treatment.

Based on the need for accurate temperature measurements during ultrasound hyperthermia, the development of an accurate, safe, and high speed thermometry system was the main goal of this study.

1.2 Background of ultrasound hyperthermia thermometry system

1.2.1 Thermocouple theory

Before developing a new thermometry system, it was necessary to review the basics of thermocouple characteristics and measurement techniques. Any segment of any conductor produces a Seebeck thermoelectric potential due to the Seebeck effect [17] which is given by,

$$dE=\alpha_A \, dT \, , \tag{1}$$

where

α_A: is the absolute Seebeck coefficient (or thermoelectric power) of material A,

dT: is the differential temperature across the short segment of conductor A, and

dE: is the resulting differential Seebeck emf.

The total Seebeck emf of a segment of a conductor between points 1 and 2 can then be obtained by integration,

$$E_{12}=\int_{T_1}^{T_2} \alpha_A \, dT \tag{2}$$

Here, T_1 and T_2 are the temperatures at the ends of the segment of the conductor and E_{12} is the Seebeck emf across the segment of the conductor.

An open circuit thermocouple is formed by joining two dissimilar metal wires (metal A and metal B) at one end and leaving the other ends of the two wires open as

in Figure 1.1.

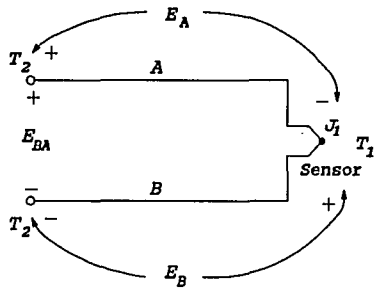

Figure 1.1 Thermocouple circuit of metal A and B

A relative Seebeck emf is established when the joined junction is being held at temperature T_1 and the two open ends are held at temperature T_2 [15,17]. Based on the Seebeck emf given in eqn (2), the relative Seebeck emf of material A and B can then be expressed as the following,

$$-E_{BA}=\int_{T_2}^{T_1}\alpha_B\ dT+\int_{T_1}^{T_2}\alpha_A\ dT \qquad (3)$$

$$-E_{BA} = \alpha_B(T_1 - T_2) + \alpha_A(T_2 - T_1)$$

$$E_{BA} = (\alpha_A - \alpha_B)T_1 - (\alpha_A - \alpha_B)T_2$$

$$E_{BA} = \alpha_{A\text{-}B}(T_1 - T_2),$$

where

$\alpha_{A\text{-}B}$: is the relative Seebeck coefficient (or thermoelectric power) of metals A and B.

Using a volt meter to measure voltages across a thermocouple, e.g. copper-constantan (a thermocouple made from copper wire and constantan wire), the equivalent circuit can be shown as Figure 1.2 (where the volt meter terminals are usually made from copper).

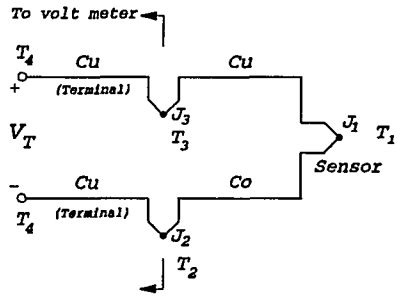

Figure 1.2 Thermocouple voltage measurement

In Figure 1.2

Co indicates the constantan (alloys of copper and 35% to 50% nickel) lead and

Cu indicates the copper lead.

Assuming that both terminals of the voltmeter are at the same temperature (T_4) and that all Cu leads have the same Seebeck coefficient (i.e. the differences in these materials is neglected). Then, V_T read by the volt meter can be written as:

$$-V_T=\int_{T_4}^{T_2}\alpha_{Cu}\ dT+\int_{T_2}^{T_1}\alpha_{Co}\ dT+\int_{T_1}^{T_3}\alpha_{Cu}\ dT+\int_{T_3}^{T_4}\alpha_{Cu}\ dT$$

$$-V_T = \alpha_{Cu}(T_2 - T_4) + \alpha_{Co}(T_1 - T_2) + \alpha_{Cu}(T_3 - T_1) + \alpha_{Cu}(T_4 - T_3)$$

$$-V_T = \alpha_{Cu}(T_2 - T_1) + \alpha_{Co}(T_1 - T_2)$$

$$V_T = \alpha_{Cu\text{-}Co}(T_1 - T_2) \quad (4)$$

In order to measure the relative temperature change between junction J_1 and junction J_2 in Figure 1.2, junction J_2 is held at a known reference temperature, T_{ref} (i.e. an ice bath or a known temperature isothermal block (see Figure 1.3)) and the equation for V_T becomes,

$$V_T = \alpha_{Cu\text{-}Co}(T_1 - T_{ref}). \quad (5)$$

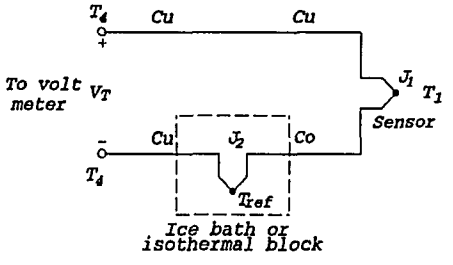

Figure 1.3 Reference junction compensation

When both thermocouple metals are different from the volt-meter terminals, e.g. manganin-constantan, as shown in Figure 1.4, then junctions J_2 and J_3 should be held at the same temperature for easier measurement of the relative temperature of junction J_1 to the reference temperature T_{ref}.

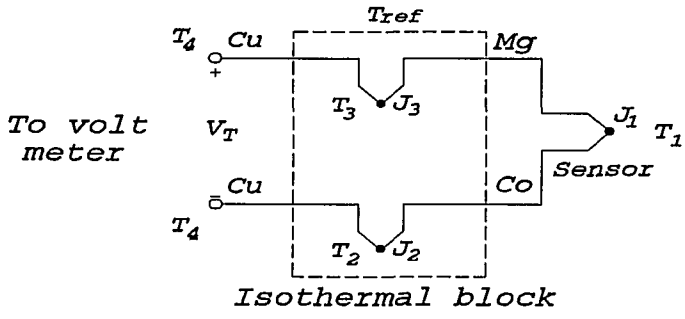

Figure 1.4 Equivalent reference junction arrangement

In Figure 1.4, both copper wires are assumed to be the same and Mg labels the manganin lead. The resultant V_T can be derived as,

$$V_T = \alpha_{Cu}(T_4 - T_2) + \alpha_{Co}(T_2 - T_1) + \alpha_{Mg}(T_1 - T_3) + \alpha_{Cu}(T_3 - T_4).$$

If $T_{ref} = T_2 = T_3$, then

$$V_T = \alpha_{Mg\text{-}Co}(T_1 - T_{ref}) \qquad (7)$$

Thus, from the result of eqn (7), the temperature of junction J_1 can be obtained by measuring V_T, and knowing both $\alpha_{Mg\text{-}Co}$ and the reference temperature T_{ref}.

1.2.2 Artifact

A thermocouple is not a perfectly invisible sensor to ultrasound. Generally, there are three temperature measurement artifacts associated with ultrasound hyperthermia treatments [5]. The first artifact is the viscous heating artifact due to the relative movement of the surrounding material and the probe. This causes an energy absorption at the probe/tissue interface and produces a temperature elevation [6, 7].

This effect occurs as a transient temperature in the probe when an ultrasound impulse is applied. The second artifact is caused by the fact that in patients the probe has a plastic sheath around it. Plastic is a better ultrasound absorber than the surrounding tissue and thus a large temperature elevation occurs when an ultrasound impulse is applied [5, 10]. This effect causes a higher temperature elevation than the viscous heating effect. The third artifact is caused by the physical existence of the probe in the ultrasound field which causes a wave reflection and scattering from the probe. This causes an increased power density (power deposition from both the direct and reflected waves) near the probe's surface when the ultrasound beam's shape has changed due to the different acoustical impedances between the probe and its surrounding tissue [5]. However, if the dimension of the probe is less than 1/3 of the wavelength, the field disturbance becomes insignificant [5]. In patient treatments, the three artifacts are minimized by temporarily turning off the power for 3 s during scanning before the temperatures are measured [25]. Turning the power off allows the ultrasound to not impinge directly on a sensor during the measurement time. On the other hand, the existence of an artifact on these probes can be used to our advantage to locate the individual sensors while pulsing the ultrasound. This will be discussed in detail in Chapter 4.

1.2.3 Isolation

Electrical isolation of medical equipment is needed to provide safety to the patient during treatments. Figure 1.5 shows a simple set up for two basic leakage

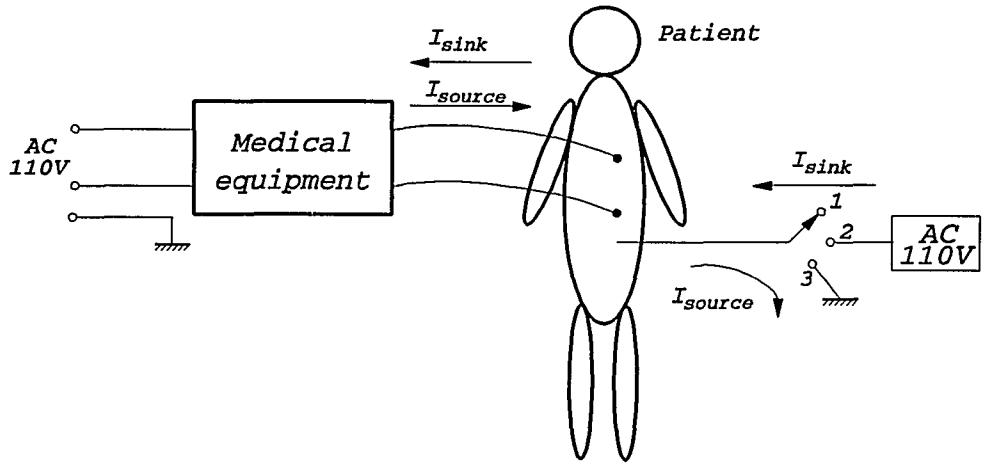

Figure 1.5 Simplified patient electrical safety with medical equipment

current measurements in electrical safety protection for the patient. The I_{sink} leakage current specification (20 μA) must be met in order to protect the patient from accidents involving a the 110 V power line (switch closed at position 2) when the patient is in direct contact with the power line. The I_{source} current specification (10 μA) is required to protect the patient from leaky equipment. One example of this leakage is if the

patient is in direct contact to the earth ground (switch closed at position 3) while a leakage from the primary 110 V power line in the equipment to the patient body is occurring [18, 19, 20].

Isolation is achieved in the UACC thermometry system used during SFUS treatments by using polyethylene tubing encased thermocouple sensors during patient treatments. As discussed in Section 1.2.2, artifacts are introduced during temperature measurements when a polyethylene tubing thermocouple probe is used. This artifact could hinder the thermometry system from reading accurate temperature measurement during the treatment. In order to meet the safety aspects for medical applications, equipment isolation is needed.

Another reason to isolate a thermometry system for ultrasound hyperthermia is to reduce the earth ground noise, due to noisy equipment, to the thermocouple measurement equipment input when bare probes are used during animal experiments. Bare probes are used during animal experiments because minimum artifacts can be achieved. In some experiments, the animal is placed in direct contact with the water bath (which is usually earth grounded) to have the beam directly impinge onto the animal for effective heating and precise data collection. In this situation leakage current through the earth ground is measured by the thermometry system. The solution used for a non-isolated thermometry system to this noisy ground is to use fused silica tubing which has a lower artifact compared to the polyethylene tubing to isolate the probe from earth ground. However, this is not a preferred method for experiment because artifacts

are still a problem during experimental data collection. Thus, it is also needed to isolate the thermometry for animal experiments.

The basic technique used in medical equipment is to use an isolation component to isolate the front stage equipment (direct contact with the patient) from the rear stage equipment (non-direct contact with the patient). The isolation component choices available for signals in medical equipment are an isolation amplifier which can be used for analog signals and an opto-isolator which can be used for digital signals [21]. These isolation components are then powered by an isolated power supply which is separated and isolated from the non-isolated end of the rear equipment power supply. Isolation amplifiers usually yield an output drift temperature coefficient in the range of a few millivolts per °C and a relatively slow settling time of a few milliseconds. On the other hand, opto-isolators which isolate digital signals are available with a relatively large bandwidth of up to 10 MHz. The temperature drift of the opto-isolator is not a significant factor since only digital signals are involved.

1.2.4 Speed of temperature acquisition

An existing, fast speed isolated thermometry system, made by Lifetec Pty. Ltd, reads temperatures at a speed of 128 sensors per second. However, for a multi-sensor thermometry system to measure transient temperatures from 112 sensors, a higher speed thermometry system is needed to measure transient temperatures during treatment.

1.3 Previous thermometry system at UACC

The thermometry system used for the past seven years for ultrasound hyperthermia was able to read temperatures from up to 112 sensors. This system consisted of an HP-computer (model HP9836) to control the system, an HP-DVM (model HP3456A) that measures thermocouple voltages, an HP data acquisition unit (model HP3497A) that selects the thermocouple sensor to be measured, and a connector box that interfaces the probe to the data acquisition unit. A system diagram of this set up is shown in [11]. This system can take temperature readings at a maximum speed of approximately 40 ms per sensor [14]. It takes approximately 2.24 s to complete one reading of eight probes with seven sensors on each probe. This slow reading speed could lower the temperature scan rate significantly during temperature measurements when the total number of probes is increased. This could cause temperature information losses over a long time delay during experiments and even treatments. Also, the locate routine (to be discussed later) which measures the transient temperature can only search for one sensor during each execution. It would therefore take 56 executions of the locate routine to locate all sensors on 8 probes. In addition, the equipment used in this system is not electrically isolated and, therefore does not satisfy the safety requirements for medical use when bare (non-insulated) probes are involved. The isolation for this system has been achieved by using polyethylene or fused silica thermocouple probes, which both produce artifacts, during human treatment or animal experiments, respectively. Thus, there was a need to improve this thermometry system

in terms of speed and isolation with bare probes.

1.4 Improved thermometry system

The new thermometry system was designed and developed primarily to overcome the speed and electrical isolation limitations of the existing thermometry system when measuring transient temperatures from multi-sensor probes and to reduce artifact during temperature measurement. This new system can measure 16 probes with 7 sensors on each probe in approximately 0.2 s with a single scan. With this reading rate, a complete search for all sensors on 16 probes is possible in one execution. Also, electrical isolation has improved to a leakage sink current of 75 μA at 110 V AC at 60 Hz while satisfying the leakage source current of 10 μA. This thesis will discuss in detail the description of the new thermometry system hardware and the hardware performance evaluation in Chapter 2, the temperature measurement techniques used and the algorithms to obtain the desired system accuracy in Chapter 3, the multi-sensor location search method and its' reliability in Chapter 4, and a discussion of this system with suggestions for future work in Chapter 5. For ease of operation, a user friendly interface with window driven menu, was incorporated into the system software (Appendix E). In addition, a second version of the system which reduced in size, leakage current, and equipment temperature coefficient is documented in Appendix C.

CHAPTER 2

HARDWARE DESCRIPTION

2.1 System hardware setup

The thermometry system hardware is depicted in Figure. 2.1 which shows the 386-20 MHz personal computer that controls the entire system's operation. The peripheral devices which comprise the rest of the temperature measurement system are a bus buffer card, an opto-isolation unit, and a temperature acquisition unit. The bus driver buffer card provides digital signal buffering via a line driver from the computer to the external devices. The opto-isolation unit isolates the front stage equipment which comes in direct contact with the patient from the 60 Hz main power supply. This isolation unit provides electrical isolation for the system to satisfy the requirements for clinical safety according to UL544 [18] (also refer to [19], [20]). The temperature acquisition unit (TAU) reads and amplifies voltages from the thermocouple sensors, and then performs an A/D conversion of the thermocouple voltage into digital signals for the PC. Details of the bus driver buffer, opto-isolator and temperature acquisition unit will be discussed in their respective sub-sections.

The main purpose of the PC and the temperature acquisition unit is to achieve data communication between these two units. The opto-isolation unit is an intermediate step between the computer and the temperature acquisition unit to perform opto-isolation and still faithfully transfer signals between the two components. Three types of buses are involved in this communication: the address bus, the data bus, and the control bus. The 14-bit address bus is used by the computer to interface to the temperature acquisition unit. The addresses can be grouped into a base address (Hex250 to Hex25F that requires the address line A_0 to A_9) and a sub-address (A_{10} to A_{13} or an incremental order in address location of Hex400). The base address is used to select the temperature acquisition unit and the sub-address is used to select the specific thermocouple probe and sensor. The TAU 8-bit data is sent back to the computer on an 8-bit data bus. The control bus consists of four control signals that are used to provide hand shaking: IOR (I/O read), AEN (address enable), I/O CHRDY (I/O channel ready), and RESET.

2.2 Bus driver buffer

The bus driver buffer unit is an expansion card that plugs into the PC expansion slot to buffer and drive address lines and control lines to the opto-isolation unit when long cabling is used for data transmission (the detailed circuit schematic is in Appendix A.1). This includes address lines from A_0 to A_{13}, and control lines IOR, AEN and

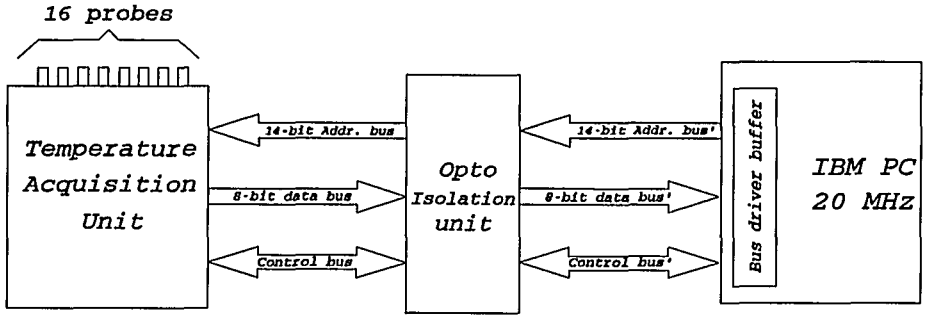

Figure 2.1 Thermometry System block diagram

RESET. With this bus driver buffer, the PC expansion bus is protected from external loading produced by the long cable which would introduce inductive (noise pick up) and capacitive effects (add on shunt impedance causing current bypass) along the transmission lines to the opto-isolation unit.

Open-collector drivers (74LS17) are used on this card to provide the above function. Each output of the driver is connected to a 270 Ω pull up resistor at +5 V to provide sufficient current (approximately 18 mA) to drive the signal to the receiving end of the cable. The output of the line driver is always active (i.e. output is either logical high or low, no tri-state can occur), since there is not multiple output signals

connected to a single input of the opto-isolator.

2.3 Temperature Acquisition Unit

This unit, as depicted in Figure 2.2, measures the thermocouple voltages and converts them into a digital signal. The unit consists primarily of eight amplifier cards with two multi-sensor (7 sensors) channels on each card, and a card select and pulsing card. The amplifier cards amplify the low DC thermocouple analog signals into larger DC voltages and convert the amplified analog signals into a 12-bit digital signal for computer processing [16]. The card select and pulsing card selects one amplifier card at a time in order to read a single sensor's 12-bit digital signal from the selected amplifier card, and sends the 12-bit signal out as two 8-bit signals to the PC. Details of the address technique and control signals for the TAU are discussed in a sub-section of this chapter.

2.3.1 Amplifier card

The amplifier card shown in Figure 2.3 has an instrumentation amplifier, a multiplexer, a unity gain buffer, an A/D converter, and a current source circuit. The instrumentation amplifier amplifies the thermocouple input DC voltage by 1000 times. This amplified signal is then multiplexed by the multiplexer which selects a sensor from one of the two probes on the selected card. The unity gain buffer prevents loading of the multiplexer output from the A/D converter that converts the analog DC voltage to

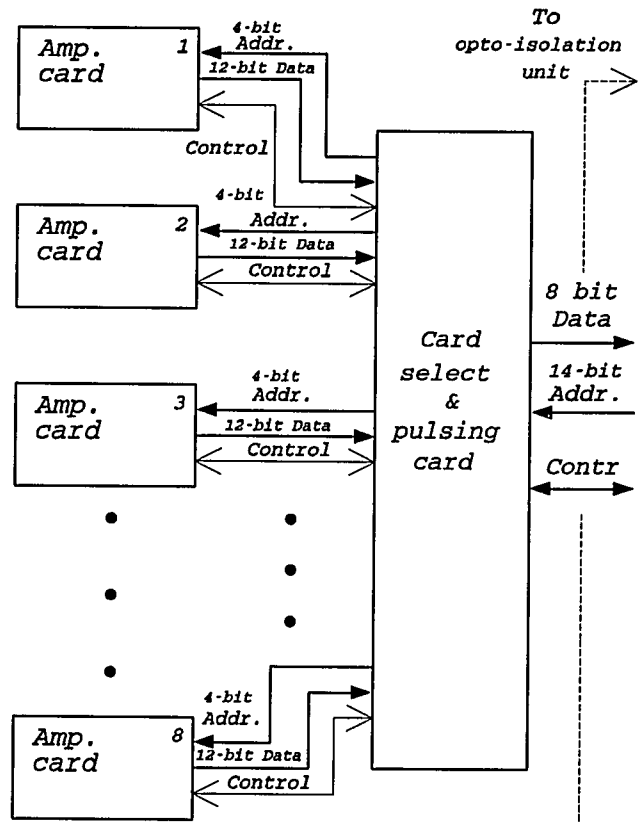

Figure 2.2 TAU block diagram

a 12-bit digital signal. The current source circuit provides a constant current to a thermistor whose voltage is then multiplexed and converted by the A/D converter for the reference junction temperature measurement.

2.3.1.1 Functional description of amplifier and A/D converter

Each amplifier card contains fourteen high gain (x1000), low temperature input offset drift (maximum of ± 5 μV/°C), low gain drift (5 ppm/°C), low quiescent current (750 μA) and high CMRR (common mode rejection ratio, 90 dB) instrumentation amplifiers (Burr-Brown, INA102KP) to boost up the DC voltage of the thermocouple sensor by 1000 times. The typical voltage range of a T-type thermocouple, when the reference junction temperature is at ambient temperature (24 °C), for temperatures from 20 °C to 60 °C is approximately -160 μV to 1.5 mV. With a gain of 1000 on the front stage amplifier, the amplified thermocouple voltage range becomes -0.16 mV to 1.5 V. The gain drift is insignificant in this application; however, the input offset drift is rather significant for this application and the compensation method for this drift will be discussed in Chapter 3. Two biasing resistors as recommended by the manufacturer are used at each terminal of the front stage amplifier input to provide a bias current return path for the thermocouple input as shown in Appendix A.4 such that an open circuit or an unbalanced input does not occur. Two coupling capacitors in parallel with the biasing resistors are connected on each input terminal of the amplifier. They act as an

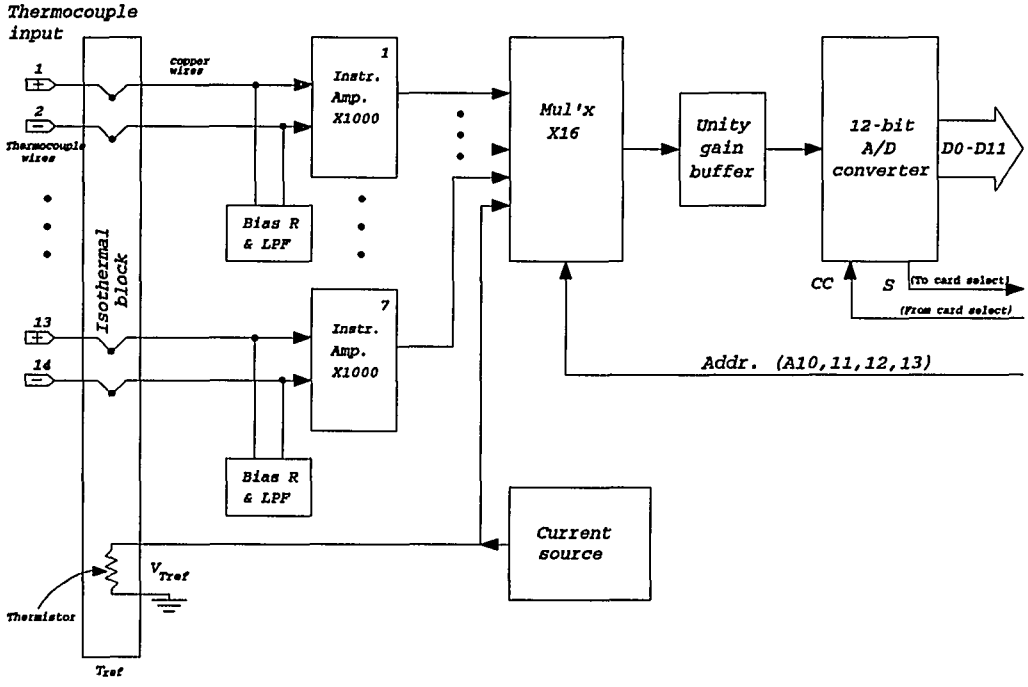

Figure 2.3 Amplifier card block diagram

RC LPF (low pass filter) to filter out noise at frequencies higher than 1.6 Hz that are picked up by the input of the thermocouple. However, this RC LPF has a response of $V_o = V_{in}(1-e^{-t/RC})$ for a step signal, where V_{in} is the actual thermocouple voltage and V_o is the measured thermocouple voltage upon the step (e.g. If $V_{in}=10\ \mu V$, then at time $t=0.2$ s; $V_o=8.6\ \mu V$). From the step response, the RC LPF does reduce the actual transient temperature measurement but it still provides sufficient information of the relative transient temperatures during the sensor location search routine, which will be discussed in Chapter 4. Each amplifier output is then connected to the input of a 16-channel multiplexer. The amplifier output signal is selected by the combination of sub-address lines A_{10}, A_{11}, A_{12} and A_{13} from the PC, provided that the temperature acquisition unit base address is selected. The base addresses ranges from Hex250 to Hex25F. A detailed memory map for the temperature acquisition unit is shown in Table 2.1.

A 16 channel single-ended CMOS analog multiplexer (Burr-Brown, IH-506A-5) which has a maximum access time of 1 μs is used to select thermocouple sensors and reference junction measurements. This 1 μs access time is taken care of by the pulsing circuit of the card select and pulsing card which will be discussed in Section 2.3.2. Out of the 16 channels on the multiplexer, only 14 channels are used for the two thermocouple probes on each card with 7 sensors on each probe. The other two remaining channels on the multiplexer are used for selecting the reference junction

	Card1	Card2	Card3	Card4	Card5	Card6	Card7	Card8
Tref1a	H250 H251	H252 H253	H254 H255	H256 H257	H258 H259	H25A H25B	H25C H25D	H25E H25F
sens1a	H650 H651	H652 H653	H654 H655	H656 H657	H658 H659	H65A H65B	H65C H65D	H65E H65F
sens2a	HA50 HA51	HA52 HA53	HA54 HA55	HA56 HA57	HA58 HA59	HA5A HA5B	HA5C HA5D	HA5E HA5F
sens3a	HE50 HE51	HE52 HE53	HE54 HE55	HE56 HE57	HE58 HE59	HE5A HE5B	HE5C HE5D	HE5E HE5F
sens4a	H1250 H1251	H1252 H1253	H1254 H1255	H1256 H1257	H1258 H1259	H125A H125B	H125C H125D	H125E H125F
sens5a	H1650 H1651	H1652 H1653	H1654 H1655	H1656 H1657	H1658 H1659	H165A H165B	H165C H165D	H165E H165F
sens6a	H1A50 H1A51	H1A52 H1A53	H1A54 H1A55	H1A56 H1A57	H1A58 H1A59	H1A5A H1A5B	H1A5C H1A5D	H1A5E H1A5F
sens7a	H1E50 HIE51	H1E52 H1E53	H1E54 H1E55	H1E56 H1E57	H1E58 H1E59	H1E5A H1E5B	H1E5C H1E5D	H1E5E H1E5F
tref2b	H2250 H2251	H2252 H2253	H2254 H2255	H2256 H2257	H2258 H2259	H225A H225B	H225C H225D	H225E H225F
sens1b	H2650 H2651	H2652 H2653	H2654 H2655	H2656 H2657	H2658 H2659	H265A H265B	H265C H265D	H265E H265F
sens2b	H2A50 H2A51	H2A52 H2A53	H2A54 H2A55	H2A56 H2A57	H2A58 H2AE9	H2A5A H2A5B	H2A5C H2A5D	H2A5E H2A5F
sens3b	H2E50 H2E51	H2E52 H2E53	H2E54 H2E55	H2E56 H2E57	H2E58 H2E59	H2E5A H2E5B	H2E5C H2E5D	H2E5E H2E5F
sens4b	H3250 H3251	H3252 H3253	H3254 H3255	H3256 H3267	H3258 H3259	H325A H325B	H325C H325D	H325E H325F
sens5b	H3650 H3651	H3652 H3653	H3654 H3655	H3656 H3657	H3658 H3659	H365A H365B	H365C H365D	H365E H365F
sens6b	H3A50 H3A51	H3A52 H3A53	H3A54 H3A55	H3A56 H3A57	H3A58 H3A59	H3A5A H3A5B	H3A5C H3A5D	H3A5E H3A5F
sens7b	H3E50 H3E51	H3E52 H3E53	H3E54 H3E55	H3E56 H3E57	H3E58 H3EE9	H3E5A H3E5B	H3E5C H3E5D	H3E5E H3E5F

Base address = H250 to H25F
(for example sensor1a: low byte = H250, high byte = H251)

Table 2.1 TAU memory map

temperature of each thermistor. These temperatures are used for the reference junction compensation, which will be discussed in Section 2.3.1.2. The multiplexer output is then connected to a unity gain buffer which has a low input offset voltage temperature drift (10 μV/°C), and then to an operational amplifier (NS, LF411N) to prevent loading from the multiplexer output to the A/D converter input of the subsequent stage.

A 12-bit bipolar A/D converter (Burr-Brown, ADC80MAH-12) with a temperature coefficient for total drift accuracy of $\pm$23 ppm/°C is used to convert the amplified thermocouple signal, which is an analog DC voltage, to a 12-bit digital signal. The input analog range of the A/D converter is configured to -2.5 V to +2.5V over it's 12-bit conversion range. Thus, the 12-bit A/D converter provides a resolution of 1.22 mV for this thermometry system. This means that with a gain of 1000 and a thermocouple output of 40 μV/°C that a maximum temperature resolution of 0.033 °C is achievable. The total time required for each 12-bit conversion is about 25 μs. The A/D converter begins its conversion only after it receives a convert command (CC), which is a positive pulse to trigger its conversion circuit (refer to the timing diagram in Figure 2.6). After a 186 ns delay from the positive triggering edge of the convert command, the A/D converter generates a signal called conversion status (S). This signal is pulled high by the A/D converter to notify the external circuitry that the A/D converter is busy. This status signal is sent to the card select and pulsing card by each amplifier card to make a combined handshake signal which is sent to the PC to indicate the TAU status and will be discussed in detail in Section 2.3.2.

2.3.1.2 Reference junction measurement

A constant current source circuit has been designed and is shown in Figure 2.4. This circuit consists of a 3.6 V zener diode (SK3A6), which has a temperature coefficient of -0.065%/°C, a general purpose PNP transistor (2N4402), and a biasing circuit, which consists of two resistors. This circuit is designed to provide a constant current source to a 1 kΩ (at 24 °C) thermistor (Beta 1K2A1) which has a temperature rating of 1 mW/°C. The thermistor is located at the isothermal block of the reference junction to measure the reference junction temperature. The constant current passing through the thermistor is designed to be a low value such that the thermistor does not heat up during measurement. The constant current is calculated from the following equation,

$$V_Z = V_{EB} + R_E * I_{const.}$$

Substituting 3.6 V for V_Z and 0.7 V for V_{EB} yields

$$3.6\ V = 0.7\ V + R_E * I_{const.}$$

For a 1 mW/°C dissipation on the thermistor at 24 °C and specifying the current passing through the thermistor to be 1 mA (approximate $I_E = I_C$), the resistor R_E value can than be calculated as,

$$R_E = \frac{3.6V - 0.7V}{I_{const}}$$

$$R_E = \frac{2.9V}{1mA} = 2.9K\Omega.$$

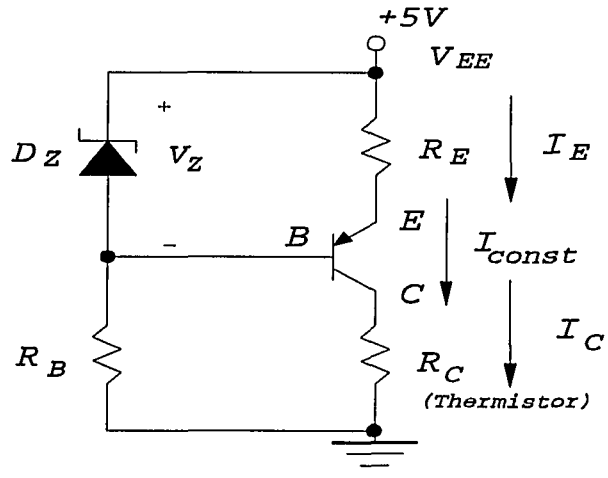

Figure 2.4 Constant current source circuit

For convenience, choose R_E to be 2.7 KΩ which is available off the shelf and provides a constant source of approximately 1.07 mA. However, for accurate measurement of the reference junction temperature, each I_{const} through each thermistor is measured and stored in a data file to be retrieved during temperature measurement (which will be discussed in the later part of this section).

The current source circuit is a temperature compensated design. When the temperature of the circuit increases, the base to emitter voltage V_{EB} tends to decrease which causes the emitter current I_E to increase. This temperature drift can be compensated by choosing a zener diode with a negative voltage temperature coefficient.

The decrease of the zener voltage lowers the voltage across the transistor base to V_{EE} and approximately sustains a constant current flow into the transistor emitter when V_{EB} is reduced as the temperature increases. A general calculation of the constant source drift with temperature can be expressed as the follows. Assume the resistance R_E is constant (insignificant temperature drift, 50 ppm/°C) within a temperature range of 24 to 32 °C. As the temperature increases by 1°C, the zener voltage is reduced by 0.065% or 2.34 mV and V_{EB} is said approximately reduced by 2 mV. Then, the changes in I_{const} will be -0.13 μA. Thus, changes of I_{const} will cause an error reading of the thermistor resistance by less than -0.13 Ω. Converting the resistance error of the thermistor reading to an error in temperature (approximately 35 to 40 Ω/°C), the reference temperature error will become +0.003 °C which is insignificant in this application. However, in actual application, the reliable temperature range of the constant current source also highly dependents on the beta (ß) value of the transistor and the current flow at the zener break down point. For this temperature compensated circuitry in this thermometry system, constant current with low temperature drift factor is supplied to the thermistor for room temperatures of 24 to 32 °C, which maintains an accuracy of ±0.02 °C for the thermistor measurement.

The thermistor voltages are read during each thermocouple acquisition cycle. This voltage is multiplexed and measured by the A/D converter. The thermistor (whose resistance is a sensitive function of temperature) is used as a temperature sensor to detect the temperature changes in the isothermal block. This thermistor temperature

is read as the reference temperature for the thermocouple sensors as shown in Figure 2.3, which corresponds to the junctions that are established where the thermocouple wire changes to copper on the amplifier card. Any changes which do occur are noted as reference junction temperature changes and are compensated for in the software. To assure accurate measurement of the reference temperature, each thermistor is calibrated against a precision reference thermistor in a stable water bath.

The calibration procedure for thermistors was conducted by inserting the thermistors and a precision reference thermistor into a 4-hole aluminum cylinder which resides in a well stirred stable water bath. These four holes of the aluminum cylinder were filled up with water to their rim to establish stable thermal flow in the holes. Energy was conducted from the water bath to the aluminum cylinder and into the four holes where the calibration thermistors and reference thermistor were situated. The maximum temperature fluctuations inside these holes were found to be ± 0.01 °C within a period of 15 s. Any other slow time varying temperature fluctuations are not considered in this case. The resistance of all the thermistors being calibrated and the precision reference thermistor were measured by a precision 6-digit multi-meter. Calibrated data provided by the National Bureau of Standards for the precision reference thermistor (Thermometric inc., model s10, serial number TM113) was used to convert the reference thermistor's resistance to temperature. This gave an accuracy of ± 0.01 °C. All thermistors were calibrated at three temperatures (20, 25, and 30°C) which spans the temperature range over which the thermistors were expected to operate.

The constant current source passing through each thermistor was obtained from measuring the resistance and the voltage across each thermistor on each amplifier card by the multi-meter. Data for the current and the curve fitting coefficients for each thermistor are shown in Appendix B.

2.3.2 Card select and pulsing card

The card select and pulsing card consist mainly of 12 8-bit data driver buffers that buffer and drive the selected data from the amplifier card data to the PC, a pulsing circuit that generates a convert command to the amplifier card A/D converter, a PC hold circuit to handshake with the PC during a temperature read operation, and an 8-channel multiplexer with logic circuit to select each valid amplifier card's data one at a time as in Figure 2.5 (a detailed circuit is shown in Appendix A.3).

This card select and pulsing card also contains the base address decoder circuit of the TAU. When the address line of A_4 A_5 A_6 A_7 A_8 A_9 are tied as (101001) and the IOR line is tied low, then this card is selected. This also means that the TAU is selected. The TAU is selected at the base I/O address of Hex250 to Hex25F. Address lines A_1 to A_3 are used to select the amplifier card. Thus, these three lines are connected to the input of an 8-channel multiplexer to select one amplifier card at a time. Addresses A_{10} to A_{13} are latched by a D flip-flop such that these address lines can be sent to the amplifier card to select and read each thermocouple sensor. They

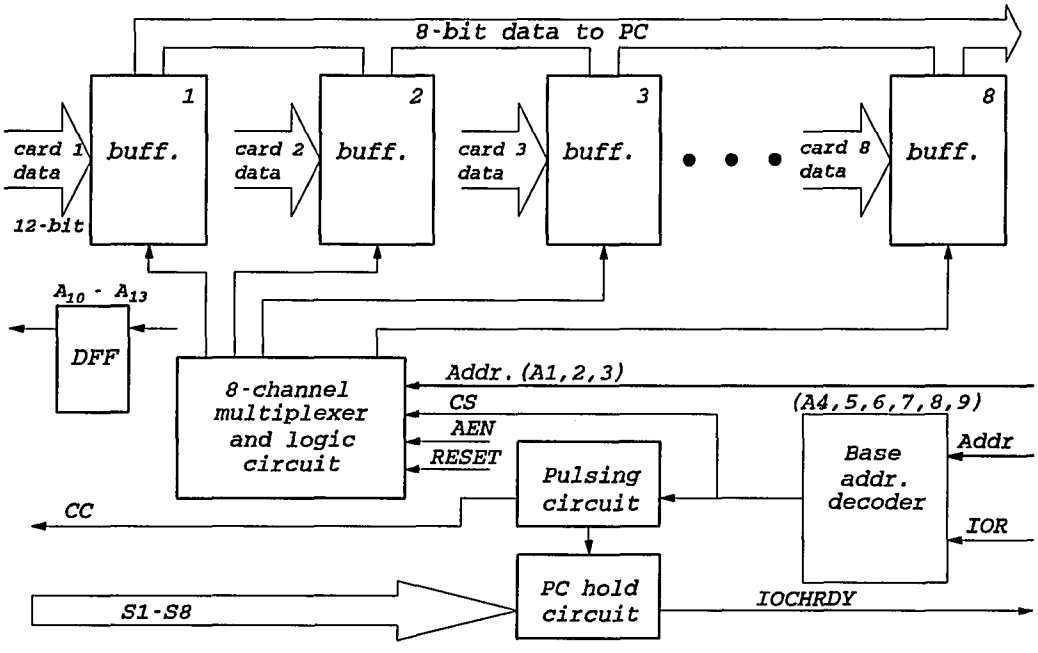

Figure 2.5 Card select and pulsing card block diagram

are latched only when the base address of the TAU is selected. This prevents the multiplexer and the amplifier card from unnecessarily switching as the PC is executing other tasks. Address A_0 is used to select the low or the high byte data from the buffer and to send the correct data byte to the PC. This address is logically ORed with the card select signal from the output of the card select 8-channel multiplexer to activate the data buffer. The buffer used in this circuit possesses a tri-state mode. The 12-bit A/D data from each amplifier card is connected directly to these driver buffers. Each amplifier card requires one and one half 8-bit buffers to accomplish the 12-bit data storage. The output of each buffer is connected to the common data bus corresponding to each data line sequence. All buffer outputs are connected in tri-state with only the selected buffer being able to place its data onto the data bus. Thus, there are no conflicts between any two buffers or amplifier cards during data transfer. The data bus is then connected to the opto-isolation unit for electrical isolation and sending data to the PC. The 12-bit data from the A/D is divided into a low byte and a high byte. The low byte carries Bits 0-7 and the high byte carries Bits 8-11 of the A/D reading, with the remaining 4-bits in the high byte ignored.

While the base address of the TAU is selected and decoded, the decoder output also triggers a pulsing circuit configured in monostable mode. The pulsing circuit can be perceived as two stages, a primary pulsing stage and a secondary pulsing stage. A timing diagram of the TAU is depicted in Figure 2.6. The decoder output is directly connected to the primary pulsing stage. When the TAU address is decoded and

Low byte:							
bit 7	bit 6	bit 5	bit 4	bit 3	bit 2	bit 1	bit 0
High byte:							
X	X	X	X	bit 11	bit 10	bit 9	bit 8

Table 2.2 12-bit A/D data storage

selected, the circuitry comprising the primary pulsing stage senses the signal and generates a positive pulse with a duration of approximately 1.74 μs. The falling edge of the primary pulse will trigger the second pulsing stage. The second pulsing stage will generate another positive pulse with a duration of approximately 1.74 μs. The second pulse is then connected to the CC (convert command) on all amplifier cards to trigger the A/D converter to begin conversion. The purpose of the primary pulsing circuit is to provide a short delay for the sub-address signals to reach the amplifier cards, to select the sensor to be read, and to allow the signal to settle (1 μs access time of the 16-channel multiplexer) before a convert command is issued to the A/D converter.

The status lines (S) from each A/D converter on the amplifier cards are logically ORed with an invertor such that the I/OCHRDY line is pulled low if any one of the status lines is pulled high. This is to ensure that all status lines have returned to the low state and that the TAU is ready to send data to the PC. The control logic of this

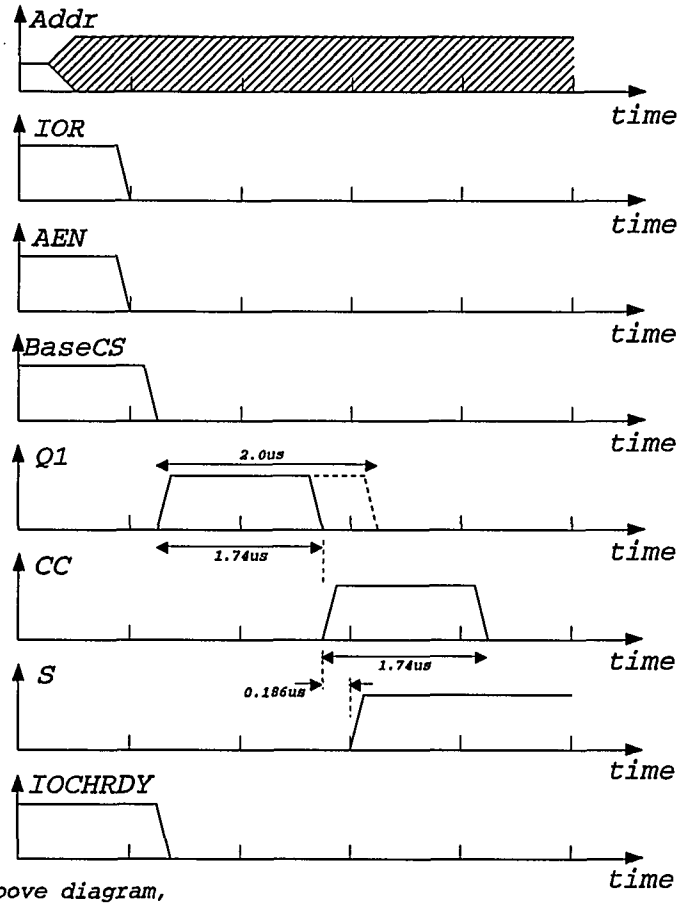

In above diagram,

Addr	*is the address signals,*
IOR	*is the I/O read signal,*
AEN	*is the address enable signal,*
BaseCS	*is the base address signal,*
Q1	*is the pulse signal,*
CC	*is the A/D conversion triggering command ,*
S	*is the A/D return status signal,*
IOCHRDY	*is the I/O channel ready signal,*

Figure 2.6 TAU timing diagram

operation is shown in Figure 2.7.

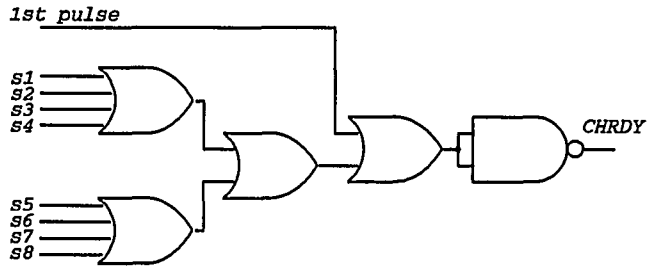

Figure 2.7 Hand shaking signal S to PC

2.4 Opto-isolation unit

The main function of the opto-isolation unit is to provide front end (patient) to rear end (main power, AC 110 V at 60 Hz and earth ground) isolation for the patient when bare probes are used during treatments, thereby satisfying the clinical safety requirement and also satisfying the accuracy requirement during animal experiments as discussed in Section 1.2.3 of Chapter 1. The opto-isolation unit mainly consists of two medical grade low leakage current (50 μA) to earth ground AC-DC isolated power supplies (computer product NFS110-7901P and NFS40-7912 approved by UL455). These supplies provide power for +5 V and $\pm$12 V to the TAU and the fourteen opto-isolator integrated circuits (HCL 2630) as shown in Figure 2.8.

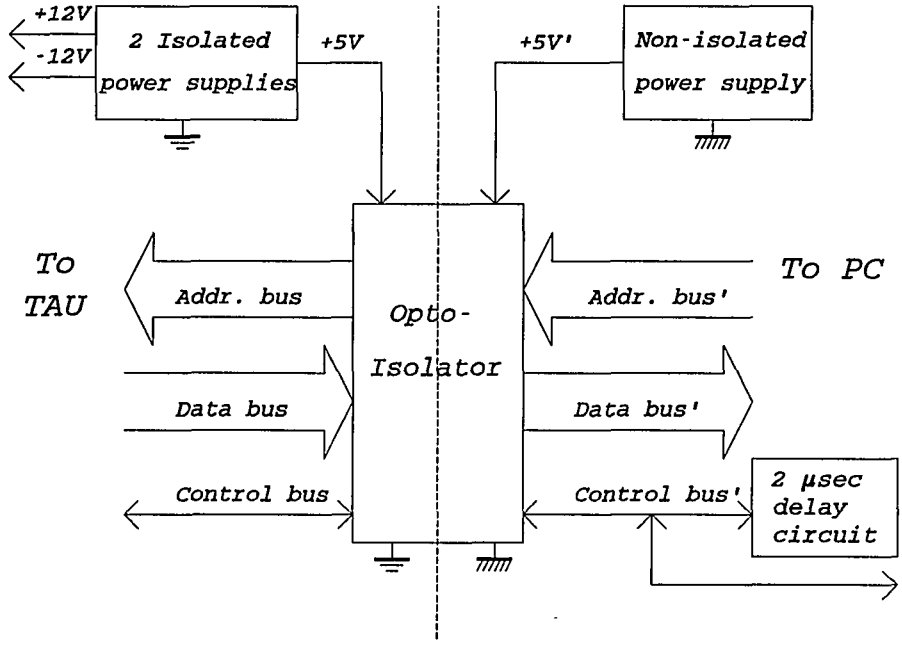

Figure 2.8 Opto-isolation unit block diagram

The opto-isolators are used to provide forward isolation for the address bus, backward isolation for the data bus, and bi-directional isolation for the control signals (a detailed circuit is shown in Appendix A.2). The rear end of the opto-isolation unit is powered by the PC power supply and the front end (patient) of this unit is powered by the two medical grade power supplies so that isolation can be achieved. Buffer/line driver devices are added to both the front and the rear end of the opto-isolation unit to provide sufficient current drive capabilities for the loading of the long distance cabling. A delay circuit similar to that of the card select and the pulsing card's pulsing circuit

was added to the opto-isolation unit. This delay circuit holds the I/OCHRDY line low for at least 2 μs when the TAU is selected as in Figure 2.6. The delay is required to allow the status signal (S) from the A/D converter sufficient time to react to the convert signal and reach the opto-isolator unit.

2.5 Hardware performance

The evaluation of the hardware performance (up to this stage) is confined to the discussion of the temperature acquisition speed and the isolation for medical safety applications of this thermometry system. The discussion of the accuracy of the temperature measurements, which involves incorporation of the calibration procedure for thermocouple probes, will be presented in Chapter 3.

2.5.1 Speed of temperature acquisition

The temperature acquisition speed of this system was tested under a program coded in Microsoft Basic 7.0. A single scan of 16 thermocouple probes which corresponds to 112 temperature sensor voltage readings with conversion to temperature values before display was found to take approximately 0.2 s. The time required to repetitively scan ten sets of data from 16 probes, with averaging of the measurements and temperature conversion before display, was found to be approximately 0.8 s. The repetitive scan of ten sets of data from 16 probes with averaging of the measurements was carried out by adding all ten measured voltages for each thermocouple sensor

before a temperature conversion was performed. This temperature reading speed has overcome the restriction of most thermometry systems which can only read a small number of sensors when transient temperatures are to be measured. With the speed of this new thermometry system, transient temperatures are able to be measured for all 16 multi-sensor (7 sensors) thermocouple probes in one execution.

2.5.2 Isolation performance

2.5.2.1 Isolation measurement

Although opto-isolation in this system provides safety protection between the TAU and the rear equipment, the system is still not safe for medical use with bare thermocouple probes. This thermometry system has satisfied the equipment leakage source current safety specification for bare probes. This safety specification measures the probe to probe leakage current, the chassis to earth ground leakage current safety, and the chassis to earth ground conductivity safety for medical use. However, this thermometry system has not satisfied the leakage sink current specification, which measures the probe to earth ground leakage current. The probe to earth ground isolation during sink current measurement must to be 20 μA or less of leakage current for AC 110 V at 60 Hz [18, 19, 20] as discussed in Section 1.2.3 of Chapter 1.

For this system, the probe to earth ground leakage sink current measured was approximately 75 μA for AC 110 V at 60 Hz. About 50 μA of this leakage current was contributed by the commercial AC-DC power supply operating at 110 V 60 Hz and

about 25 μA leakage current was contributed by the long cabling due to the leakage capacitance from the isolation unit to the TAU.

A second version of the system which has a lower leakage sink current is documented in Appendix C.

CHAPTER 3

TWO POINT CALIBRATION AND REFERENCE JUNCTION COMPENSATION

It is necessary to calibrate and compensate each probe in this thermometry system. Calibration is used to adjust the known errors of each thermocouple sensor's reading. Compensation is used to adjust the probe reading based on the environmental temperature changes during temperature measurement. Two types of compensation are involved: (a) reference junction compensation, and (b) equipment temperature drift compensation. This chapter discusses the details of the thermocouple calibration and compensation techniques, the equations used for both calibration and compensation, and the data storage format for the calibrated and compensated information. A flow chart for the temperature measurements and the results of comparisons between compensated and non-compensated measurements are presented.

3.1 Calibration technique

It is important to calibrate each thermocouple probe in each port in which it may be used. This is because each probe yields a different uncalibrated temperature reading

at the same reference junction temperature due to inhomogeneity in sensor construction, a different path through different electrical elements such as amplifiers with different initial input offsets and unmatched bias resistor values at the amplifier input (detailed circuit shown in Appendix A.4), and different resistances to the input of the amplifier through the connector pins. The general equation for significant voltage drop for the final stage of voltage measurement is shown in eqn (7).

$$V_{final} = V_{T\text{-}couple} + V_{conn} + V_{amp\text{-}ip} + V_{amp\text{-}ip\text{-}offset} \,, \qquad (7)$$

where

V_{final}: final voltage measurement

$V_{T\text{-}couple}$: thermocouple voltage

V_{conn}: voltage across connector

$V_{amp\text{-}ip}$: voltage from connector to amplifier input

$V_{amp\text{-}ip\text{-}offset}$: initial amplifier input offset.

These differences may introduce different readings on different ports for the same probe and one never knows which thermocouple will be used with which port prior to treatment. At a given temperature for uncalibrated probes, the temperature reading of thermocouple sensors measured on the new thermometry system in all ports, can have readings ranging up to ± 3 °C between each sensor. Thus, to obtain an accuracy of ± 0.05 °C (our design goal), calibration for each sensor is necessary.

3.1.1 Two point calibration

Thermocouple EMF vs actual temperature is a nonlinear curve [15]. Thus, a one point calibration cannot provide accurate temperature information if the measurement point is far away from the calibration point. The temperature obtained when using a one point calibration is usually only accurate within a limited range near the calibration point. Experimental results for manganin-constantan thermocouples using a one point calibration have been reported by Anhalt and Hynynen [14]. On the other hand, a two point curve fitting calibration technique provides additional information needed for more accurate measurements over a relatively larger range. The only unknown error is the mid range temperature. However, this unknown mid range error was found experimentally to be acceptable for use in hyperthermia treatment and will be discussed in Section 3.3. The two point calibration improvement over a wider reliable range was also verified experimentally by Anhalt and Hynynen [14]. The difference between a one point and a two point calibration for thermocouple offset and accuracy of temperature measurement is illustrated in Figure 3.1.

In Figure 3.1,

T_{probe} is the temperature calculated from the probe EMF with no offset used,

$T_{with.offset}$ is the probe temperature adjusted by an offset for the one point calibration, and adjusted by offset1 and offset2 for the two point calibration,

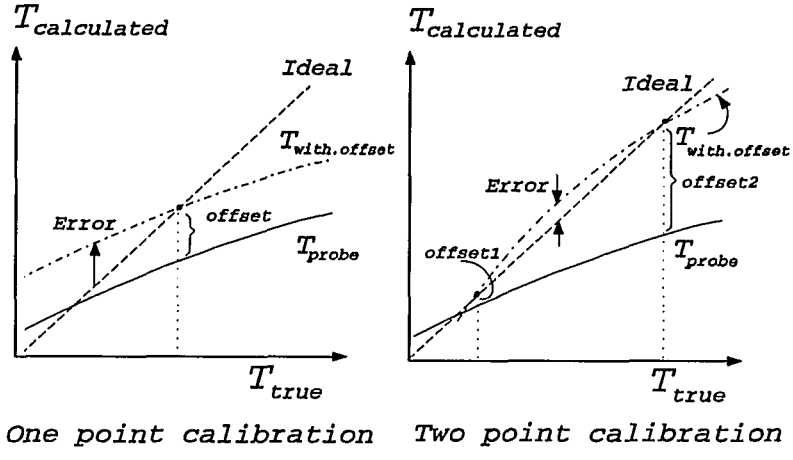

Figure 3.1 One and two point calibration offset adjustment

$T_{calculated}$ is the calculated temperature value, and

T_{true} is the true temperature value.

The previous calibration techniques carried out by the UACC on the old thermometry system used a one point calibration. With the one point calibration, the confidence level of accuracy during measurements is limited to a narrow range of temperatures near the calibration point, whereas the two point calibration provides a higher level of accuracy during measurement within a larger temperature range [14]. In order to attain the accuracy requirements of ± 0.2 °C in the 30 °C to 50 °C

temperature range set forth by the HPC (Hyperthermia Physic Center) [22] for hyperthermia thermometry, a two point calibration was implemented for this thermometry system [14].

3.1.2 Reference junction compensation

Reference junction compensation for each probe is accomplished through software. Software reference junction compensation is used instead of hardware compensation because it is easily implemented, and fewer electrical components are needed. In hardware compensation, additional electrical components are required at each amplifier input which increases the size of the TAU. The hardware compensating components would need to be placed close to the reference junction in the isothermal block, such that these temperature compensation components can correspond to the reference junction temperature change of the sensors which they are compensating and to perform the hardware compensation correctly. It also increases the biasing current at the amplifier input which could affect the reading of the thermocouple sensor, where the thermocouple sensors signals are usually very low current and very low voltage (μV) compared to that of the biasing circuit of the reference junction compensating component, if the arrangement is not appropriate. Although software compensation consumes more time than hardware compensation during each temperature conversion, with the high speed of the 386-20 MHz PC the conversion time becomes insignificant compared to the overall system cycle time. The total time for reading a single sensor

voltage and calculating the temperature is approximately 1.8 ms. With this speed of temperature acquisition, the thermometry system is capable of measuring the transient temperature of all 112 sensors in 0.2 s.

3.1.3 Equipment temperature compensation

In addition to the software reference junction compensation, thermocouple readings are compensated for the equipment temperature drift. The equipment temperature drift summary is shown in Table 3.1.

Component	Temperature coefficient
connector difference temperature	significant (-1 °C/°C)
amplifier input offset drift	significant (+/- 5 μV/°C)
amplifier gain drift	insignificant (5 ppm/°C)
unity gain buffer input offset drift	insignificant (10 μV/°C)
A/D converter drift	insignificant (+/- 23 ppm/°C)

Table 3.1 Summary of component temperature coefficients

Two main temperature sensitive components reside in this thermometry system. The first component, as discussed in Chapter 2, is the instrumentation amplifier input which has an offset drift with temperature. The second component is the temperature

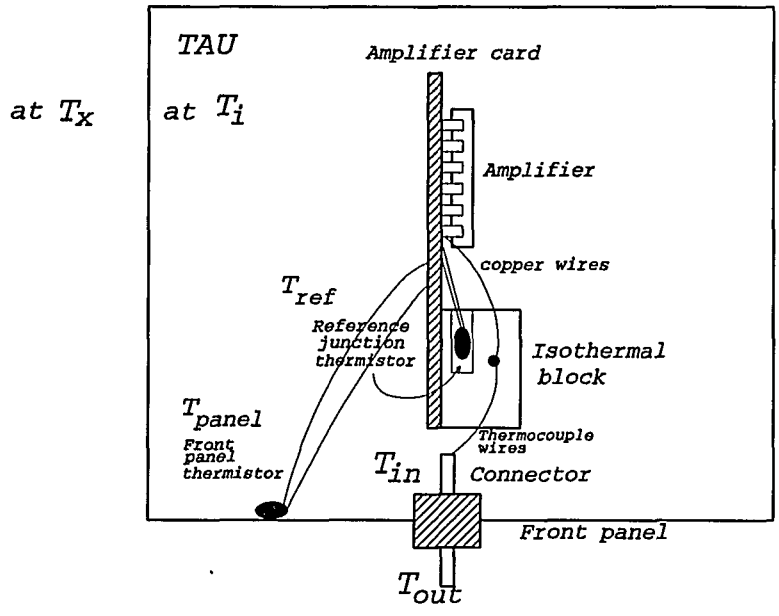

T_x :TAU external temperature

T_i :TAU internal temperature

Figure 3.2 TAU enclosure top view

difference between the outer and the inner pins of the connector which is mounted on the front panel of the TAU as shown in Figure 3.2. The difference in temperature between the outer (T_{out}) and the inner (T_{in}) connector pin of the connector will be called the temperature difference of the connector pin and is expressed as $T_{out} - T_{in}$.

A derivation of the connector effect against temperature drift of the equipment is as follows. (Figure 3.3 illustrates the equivalent circuit of the thermocouple with the connector.)

$$-V_T = \alpha_{Cu}(T_{REF}-T_2) + \alpha_{Co}(T_3-T_{REF}) + \alpha_{Cu}(T_4-T_3) + \alpha_{Co}(T_1-T_4) + \alpha_{Mg}(T_4-T_1) + \alpha_{Cu}(T_3-T_4) + \alpha_{Mg}(T_{REF}-T_3) + \alpha_{Cu}(T_2-T_{REF})$$

$$-V_T = \alpha_{Co}(T_3-T_{REF}+T_1-T_4) + \alpha_{Mg}(T_4-T_1+T_{REF}-T_3). \quad (8)$$

If $T_3=T_4$ and $T_1=T_{REF}$,

then

$V_{T1} = 0.$

If $T_3 \neq T_4$ and $T_1=T_{REF}$,

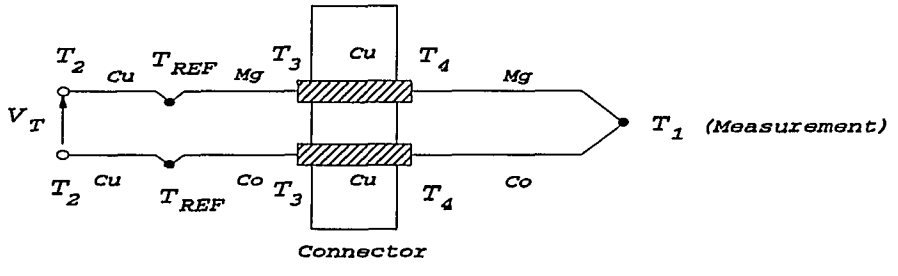

Figure 3.3 Temperature difference across connector

then

$-V_{T2} = \alpha_{Co}(T_3-T_4) + \alpha_{Mg}(T_4-T_3)$. This can be rewritten as

$V_{T2} = -\alpha_{Mg\text{-}Co}(T_4-T_3).$

The temperature drift due to a difference in the temperature at the connector becomes

$dV_T = V_{T2} - V_{T1}$

$dV_T = V_{T2} = -\alpha_{Mg\text{-}Co}(T_4-T_3).$

The above relationship is similar to eqn (4) of Chapter 1 and is equivalent to an additional manganin-constantan thermocouple sensor effect.

An experiment was set up to obtain the compensation factor for both the electrical component temperature drift (mainly amplifier input offset temperature drift) and the temperature difference across the connector. The electrical component temperature drift was measured by uncovering the TAU enclosure and varying the room temperature such that the external and internal temperature of the enclosure were held at the same temperature. This measurement was carried out with two seven sensor probes for five sets of readings (the connector pin temperature difference is at a constant value of 0 in this case) with varying room temperature. The experimental data is shown in Table 3.2.

In Table 3.2, the row "cal. at T_{ref}" gives the reference temperature inside the TAU when the TAU sensors were calibrated in a precision gallium cell at 29.772 °C, and the row "read at T_{ref}" was the reference temperature inside the TAU when the sensor readings were recorded. From Table 3.2, the temperature on each probe measured by the thermometry system yields an average relationship of approximately 1/40 °C change in measured values for each degree Celsius change the reference temperature measured at in the isothermal block, with a standard deviation of approximately 0.02 °C. The factor was obtained by averaging the values of

$$(T_{measure} - 29.772\ °C)/(\text{"}T_{ref}\text{ at reading"} - \text{"}T_{ref}\text{ at cal."})$$

over all 70 measured temperatures.

Cal. at T_{ref} (°C)	22.67	21.29	21.65	18.25	23.45
read at T_{ref} (°C)	25.32	24.11	25.03	21.82	30.02
sensor 1	29.844	29.835	29.866	29.874	29.950
sensor 2	29.823	29.809	29.847	29.894	29.935
sensor 3	29.877	29.859	29.901	29.873	29.988
sensor 4	29.851	29.841	29.875	29.858	29.957
sensor 5	29.840	29.824	29.860	29.844	29.945
sensor 6	29.849	29.837	29.874	29.845	29.958
sensor 7	29.818	29.800	29.842	29.820	29.932
sensor 8	29.869	29.857	29.892	29.863	29.977
sensor 9	29.850	29.853	29.871	29.851	29.956
sensor 10	29.811	29.807	29.851	29.816	29.937
sensor 11	29.812	29.844	29.882	29.860	29.966
sensor 12	29.829	29.832	29.848	29.831	29.936
sensor 13	29.826	29.823	29.850	29.826	29.933
sensor 14	29.859	29.851	29.882	29.860	29.937

Table 3.2 Measured temperatures for determining the temperature coefficient of the amplifiers

The compensation factor for the temperature difference of the connector was measured by supplying a thermal source (heat gun) to the front panel. The measurement was taken after the temperature difference of the connector showed a stable reading and the room temperature was held at the constant temperature such that the inner temperature of the TAU was at a constant temperature. By holding the TAU inner temperature constant, experimental data from two seven sensor probes was

cal. at T_{diff} (°C)	0.147	0.504	0.718	-0.053	-0.285
read at T_{diff} (°C)	-0.902	-0.105	-0.222	0.705	0.112
1	29.905	29.869	29.896	29.748	29.780
2	29.882	29.830	29.872	29.736	29.769
3	29.814	29.770	29.862	29.685	29.721
4	29.796	29.752	29.820	29.659	29.679
5	29.881	29.840	29.830	29.762	29.773
6	29.832	29.772	29.809	29.670	29.748
7	29.777	29.748	29.759	29.657	29.705
8	29.780	29.758	29.758	29.695	29.694
9	29.824	29.769	29.291	29.713	29.698
10	29.854	29.808	29.804	29.754	29.764
11	29.897	29.843	29.829	29.798	29.788
12	29.802	29.770	29.807	29.714	29.724
13	29.864	29.793	29.862	29.695	29.694
14	29.895	29.858	29.888	29.794	29.683

Table 3.3 Measured temperatures for approximation of temperature coefficient in connector pin difference temperature

collected as shown in Table 3.3.

In Table 3.3, the row "cal. at T_{diff}" was the temperature difference across connector when the sensors were calibrated at 29.772 °C, and the row "read at T_{diff}" was the temperature difference across connector when the sensors reading were recorded. From Table 3.3, it was found that the probe measured temperature has an average relationship of approximately 1/16 °C change for each degree Celsius change in the temperature

difference of the connector pins (which is approximated by the difference between the front panel thermistor and the reference junction thermistor temperatures) with a standard deviation of approximately 0.043 °C. The value was obtained by averaging the value of

$$(T_{measure} - 29.772\ °C)/(\text{"}T_{diff}\text{ at reading"} - \text{"}T_{diff}\text{ at cal."})$$

over all 70 measured temperatures.

The change in the measured temperature due to changes in the reference junction temperature is approximately equal to the changes in the electrical component (mainly amplifier input offset drift) characteristics within the enclosure as the temperature of the temperature acquisition unit changes. The reference junction temperature was used for the electrical component temperature coefficient compensation because it resides within the enclosure in close proximity to the electronics and, therefore, provides a relatively good indication of the electrical component temperature. The main contribution for the electrical component drift was from the amplifier input offset drift. This drift was given by the manufacturer for a worst case of 5 μV/°C. However, on an average case obtained from the above measurement, the amplifier drift was approximately 1 μV/°C in this application over a range of 8 °C change in the reference junction temperature. The temperature difference between the connector pins was approximated by measuring the temperature difference between a thermistor that measures the temperature on the inner surface of the thermal conductive front panel (aluminum) and the reference junction temperature. The measurement of the front

panel inner surface temperature was used to infer the temperature of the outer connector pin and the measurement of the reference junction temperature provided information on the inner connector pin temperature. Although this estimation was not a perfect measure of the temperature difference across the connector, it did provide a reasonable indication for the temperature difference of the connector such that accurate thermometric information could be obtained under stable environmental conditions (no external thermal source, i.e. hot or cold air, blowing directly onto the temperature acquisition unit). The temperature difference of the connector indeed was a factor of -1 °C/°C drift which was obtained from the above derivation. However, during the measurement between the reference temperature and the front panel temperature, a relation of -1/16 was found for the connector temperature difference. This was a reasonable factor to approximate the temperature difference of the connector for a range of ± 2 °C change since the approximation made for the temperature difference of the connector was not a direct measurement on the connector pin but a relation between the reference junction and the front panel temperature of the TAU, which are expected to have a larger temperature difference compared to that of the short metal pin of the connector.

3.1.4 Calibration equation

In this sub-section, the derivation of a two point calibration technique for the thermometry system is discussed. The relationship of the equipment temperature

coefficient can be approximated with the following equations.

$$\left.\frac{\partial T_{meas}}{\partial T_{ref}}\right|_{T_{diff}=const=0} \cong +\frac{1}{40}\ ^{o}C/^{o}C \tag{9}$$

$$\left.\frac{\partial T_{meas}}{\partial T_{diff}}\right|_{T_{ref}=const} \cong -\frac{1}{16}\ ^{o}C/^{o}C \tag{10}$$

In eqn (9) and (10)

$T_{diff} = T_{panel} - T_{ref}$ (for estimating $T_{out} - T_{in}$ of Figure 3.2).

For a simple case of a single point calibration (Figure 3.1) for temperature offset, the adjusted temperature measurement can be expressed as:

$$T_{offset}=T_{cal}-(T_{meas1}-\frac{(T_{ref}-24.0)}{40}+\frac{(T_{panel}-T_{ref})}{16}) \tag{11}$$

$$T_{1-adj}=T_{meas2}-\frac{(T_{ref}-24.0)}{40}+\frac{(T_{panel}-T_{ref})}{16}+T_{offset}\ , \tag{12}$$

where T_{offset}: is the offset temperature from the calibration temperature,

T_{meas1}, T_{meas2}: are the actual measured temperatures of a sensor by the system,

T_{cal}: is the calibration temperature of the sensor,

T_{panel}: is the temperature measured on the front panel,

T_{ref}: is the reference junction temperature,

T_{diff}: is the estimated temperature difference across the connector pin, and

$T_{1\text{-}adj}$: is the adjusted measured temperature of a sensor.

The term $(T_{ref}-24)/40$ is used to estimate the compensation needed for the temperature rise of the amplifier with respect to 24 °C. The relationship between the temperature measurement of the probe and the amplifier temperature changes is approximated by a directly proportional coefficient of 1/40 °C change in the enclosure internal environment temperature. The factor $(T_{panel}-T_{ref})/16$ is used to compensate for the estimated temperature rise of the temperature difference of the connector pin referenced to 0 °C of the temperature difference. This factor is needed because the relationship between the measured temperature and the temperature difference of the connector pin is proportional to -1/16. It is approximated by a coefficient of 1/16 °C for every degree Celsius change in the temperature difference. The offset temperature is calculated at a condition where the reference junction temperature is at 24 °C and the temperature difference of the connector pin is at 0 °C. This condition will be called the standard condition. This standard condition is established to provide accurate temperature calculation during temperature measurement since the calibration condition might not have the same reference junction temperature and the same temperature difference of the connector pin at the time of the temperature measurement.

Furthermore, when performing a two point calibration with a linear approximation equation, a different condition of the offset data is not informative if the two end points are calibrated and stored at different conditions. This condition is necessary because a line between the low end and the high end can not be identified. Thus, it is necessary to bring the offset to a common condition at 24 °C of the inner environmental reference temperature and at 0 °C of the temperature difference of the connector pin in order to provide a better linear approximation on a two point calibration.

From eqn (12), the two point calibration for the temperature offset is then expressed as:

$$T_{offset1} = T_{cal1} - \left(T_{meas1} + \frac{(T_{panel} - T_{ref})}{16} - \frac{(T_{ref} - 24)}{40}\right) \tag{13}$$

$$T_{offset2} = T_{cal2} - \left(T_{meas2} + \frac{(T_{panel} - T_{ref})}{16} - \frac{(T_{ref} - 24)}{40}\right) , \tag{14}$$

where $T_{offset1}$ is the low end and $T_{offset2}$ is the high end.

Fitting the two point calibration into a linear equation, the slope, a, and the constant, c, can be expressed as:

$$y = ax + c, \tag{15}$$

with a given by

$$a=\frac{(T_{offset2}-T_{offset1})}{(T_{cal2}-T_{offset2}-T_{cal1}+T_{offset1})} \quad (16)$$

and c given by

$$c = T_{offset2} - a * (T_{cal2}-T_{offset2}) , \quad (17)$$

where

y is the axis of the offset temperature,

x is the measured temperature compensated at the standard condition

a is the linear slope of the offset over the measured temperature compensated at the standard condition, and

c is the initial constant of the offset at 0 °C of the measured temperature compensated at the standard condition.

The two point calibration equation for the temperature of this thermometry system can then be obtained as,

$$T_{intmid} = (T_{meas3}+(T_{panel}-T_{ref})/16-(T_{ref}-24)/40)$$

$$T_{2\text{-}adj} = T_{intmid} + T_{intmid} * a + c , \quad (18)$$

where

T_{intmid} is the measured temperature compensated at the standard condition, and

$T_{2\text{-adj}}$ is the adjusted temperature with the two point calibration.

Thus, eqn (18) is the recovered two point calibration for this thermometry system.

3.1.5 Data storage format

The offset temperatures are measured, calculated, and stored into a database based on the above two point calibration equation. This section discusses the data storage format of the calibration and compensation information.

The two point calibration is carried out for each thermocouple probe at a low temperature (e.g. 35 °C) and at a high temperature (e.g., 45 °C) in each channel. This procedure is used to ensure that the probe will have an average accuracy of ± 0.05 °C when measuring temperatures in the calibration range (35 to 45 °C) under normal operating conditions (ambient temperature 22 °C to 28 °C) independent of the port it is used in. The calibration procedure requires information pertaining to the reference junction temperature, the difference in the temperature across the connector and the initial offset of each sensor on the probe at the calibration temperature. This information is then used to calculate and convert the probe's calibration offset data to the standard calibration conditions, a reference temperature of 24 °C with a temperature difference on the connector pin of 0 °C. The results are stored into a data file. The calibration data is stored in the following format in the data file.

probe name/connector number/high or low indicator							
calib temp	sensor1 offset	sensor2 offset	sensor3 offset	sensor4 offset	sensor5 offset	sensor6 offset	sensor7 offset

The variables have the following meaning,

probe name : is the probe's name (less then 7 characters),

connector number: is a connector number on TAU between 1 to 16, and

high/low indicator: is an indicator of H (high) or L (low) temperature.

Each calibration data storage format consists of two data types. One type is the header that holds the probe's name, the connector number in which the probe was calibrated, and the high/low calibration point indicator. Another type is the calibration data which consists of the calibration temperature, and a group of offset data for all sensors on the probe at 24 °C with a 0 °C temperature difference of the connector pin at the standard calibration condition. During calibration, a file is allocated for each probe to store its calibration data. If no file has been created for the probe, then a new file will be automatically created to store the calibration data. If the probe file does exist, only new calibration data for any connector will be appended to the existing file if the header for that particular connector does not exist. However, if the header is found in the existing file, then the new calibration data will overwrite the old calibration data for that header. All of the calibration data files and the calibration

software "ECAL" are stored under the directory "C:\dbase". The probe calibration file is searched and retrieved by the temperature measurement software.

3.2 Temperature read flow chart

A temperature read flow chart for this thermometry system is depicted in Figure 3.4.

3.3 Calibration results and accuracy

By using the two point calibration equation discussed earlier in this chapter, an average experimental error of ± 0.05 °C was obtained for 93 sensors placed in a stable water bath (which was also used for the thermistor calibration). Averaging was done for 100 readings for each sensor at several different room temperature conditions. The low end calibration temperature was 29.772 °C (precision gallium cell) and the high end calibration temperature was 52.46 °C. The difference between the compensated equipment (as discussed in Section 3.1.3) and the non-compensated equipment (ignoring the factor of 1/40 and -1/16 °C for the equipment temperature coefficient) data are shown in the following tables. Both tables incorporate two point calibration, however, the top table is not compensated for the amplifier temperature drift and the temperature difference of the connector pin.

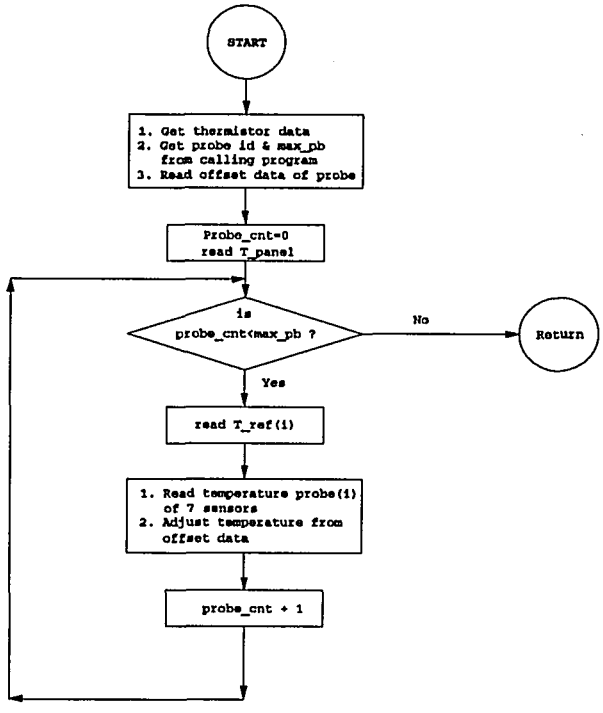

Figure 3.4 Flow chart of temperature read for probes

Temperature data collected without compensation:

T_{ref} (°C)	24.2	27.4	28.8	29.3	31.6	32.6
T_{diff} (°C)	0.7	-0.1	-0.6	-1.0	-1.8	-1.6
AVG (°C)	0.080	-0.037	-0.091	-0.060	-0.174	-0.229
SDV (°C)	0.067	0.030	0.043	0.071	0.092	0.107
Max-meas	0.23	0.03	0.01	0.01	0.04	0.05
Min-meas	-0.06	-0.08	-0.2	-0.29	-0.34	-0.49

Temperature data collected with compensation:

T_{ref} (°C)	24.2	27.4	28.8	29.3	31.6	32.6
T_{diff} (°C)	0.7	-0.1	-0.6	-1.0	-1.8	-1.6
Avg (°C)	-0.052	-0.028	-0.028	0.040	0.025	-0.084
SDV (°C)	0.067	0.034	0.045	0.066	0.100	0.120
Max-meas	0.07	0.03	0.05	0.19	0.23	0.27
Min-meas	-0.21	-0.10	-0.12	-0.17	-0.24	-0.30

Table 3.4 Temperature measurement result

In the above two tables,

AVG: is the average difference of all 93 sensor temperature readings from the actual temperature (average temperature - actual temperature), and

SDV: is the standard deviation of the 93 sensors from the actual temperature.

Although the two point calibration technique does not fully solve the thermocouple nonlinear equation, it provides a better solution than the one point

calibration technique. The measurements made within the calibration range were accurate to ± 0.05 °C under normal operating conditions. The overall standard deviation of the TAU measurement at normal operating room condition range below 30°C is 0.053 °C, and the average error range is between -0.052 °C and +0.040 °C for that same room temperature range.

CHAPTER 4

SENSOR LOCATING SYSTEM

A multi-sensor locating software routine was written to search for and to locate all of the sensors on each probe within a given x and y coordinate search area. However, the z position of each probe, which is in the direction of the focal depth of the ultrasound beam, must be predetermined by the operator before the search is conducted. Because of its slow speed, the previous thermometry system could search for only one sensor during an execution of a similar locate routine at the beginning of a treatment. The faster speed of the new thermometry system allows all sensors to be located during a single execution of the locate routine. This should improve the clinical treatments and animal experiments in terms of the more efficient use of time. This chapter will discuss the hardware set up, the search strategy, the problems encountered, and the experimental results of the new search routine.

Before further discussion of the new locate routine, it is necessary to discuss the modification of the gantry (mechanical fixture, whose movement is controlled by stepper motor, where ultrasound transducers are mounted) motor control technique for incorporation into the new thermometry system. As discussed by Anhalt [3] and

Kudrimoti [4], the original motor control of the gantry on each axis was performed by a DC comparator that compared the DC voltage of the gantry current position feedback voltage and the manual positioning potential of the destination position voltage. The voltage difference was then sent to a voltage controlled oscillator and direction discriminator to generate the necessary number of pulses to the stepper motor to move the gantry to the proper position. The single sensor search of the old thermometry system had adopted this technique to move the gantry during its search. However, this technique was sensitive to noise at the comparator which caused noise generation of unwanted pulses to displace the gantry during a search.

In Kudrimoti [4], a new technique was used to move the gantry. In this new technique, the exact number of pulses was generated by the serial port of the 386-20 MHz PC and sent to the gantry motion controller (Anaheim automation stepper motor indexers) during the SFUS treatments. This new technique was applied to control the motion of the gantry during the sensor location search on the new thermometry system. The major advantage of this technique is that it is not subject to noise interference, since the actual number of pulses required to move the gantry are sent to the stepper motor. The position error of the gantry during movement control is determined by the mechanical limitation of the stepper motor, limit switch, gears and other mechanical mounting on the gantry [3].

4.1 Hardware set up for sensor locating routine

In addition to the temperature measurement hardware (described in Chapter 2), the sensor search procedure also requires the 386-20 MHz PC serial port (RS-232) to be connected to the gantry motion controller, and the IEEE-488 interface card to be connected to a function generator (Wavetek model 271). A hardware block diagram is shown in Figure 4.1.

The connection between the PC and the gantry motion controller allows the PC to have control over each individual gantry motor (x, y, z, rotate and tilt). Rotate and tilt are not used for locating thermocouple sensors, but rather are positioned as desired by the operator prior to locating the sensors. Digital signals are sent by the PC through the serial bus to the gantry motion controller card for the x, y and z motors. The configuration between the PC and the motion controller card is as follows:

(a) Baud rate: 2400

(b) Stop bit: 2

(c) Parity bit: None

The PC sends movement commands to the motion controller card when it is performing a 2D or 3D matrix step scanning. Each pulse sent from the PC to the motion controller card is recorded by the PC in order to keep track of the current

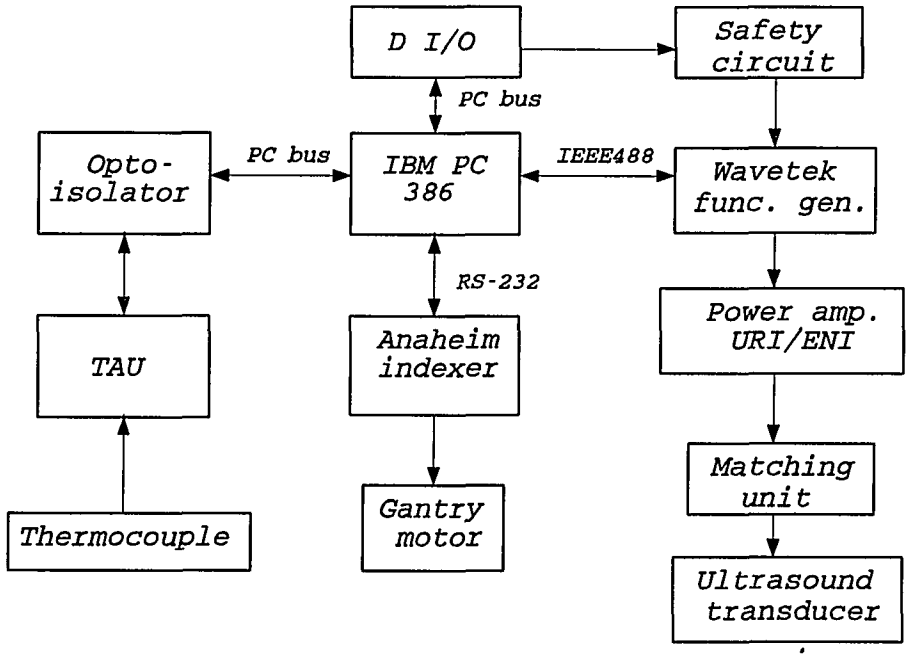

Figure 4.1 System interface to TAU

search location. Each millimeter step movement in x, y, and z requires a different number of pulses by the stepper motor. Table 4.1 shows the number of pulses required by each motor per unit of movement.

Axis	Pulse
X	16 pulse/mm
Y	17 pulse/mm
Z	70 pulse/mm
R	34 pulse/degree
T	70 pulse/degree

Table 4.1 Motor pulses (x,y,z,r,t)

The IEEE-488 card, on the PC expansion bus, allows the PC to communicate with the function generator using the IEEE-488 standard bus as the means of remote communication. Thus, the PC can have remote control of the function generator while performing the locate task. During the execution of the locate routine, bursts of RF signals are generated by the function generator which are processed by the RF amplifier before driving the ultrasound transducer. The duration of each burst is controlled by the PC by switching the function generator signal "ON" and "OFF". A list of set up commands required by the PC to communicate with the function generator are is in

Table 4.2.

Operation	Code
Frequency	F
Amplitude	A
Offset	D
Mode	B
Function	C
Burst	R
Power off/on	P0/P1

Table 4.2 Wavetek command codes

4.2 Search strategy

The multi-sensor search routine is capable of scanning a 2D or 3D matrix search by stepping the transducers through the entire search area. The most common search is the 2D search at a fixed depth selected by the operator. The search area is defined by the operator as the area where he or she believes the thermocouples will be and thus where the pulsed ultrasound signal should be focused during the search. The sensor search begins at the center of the search area where the gantry is first placed by the operator. The search proceeds by next moving to the negative corner (in the 3rd quadrant) of the search area and conducting its search toward the most positive corner

(in the 1st quadrant) of the search area in the water tank.

The search strategy relies heavily on the temperature increase recorded by the thermocouple due to an applied ultrasound field when the focus is close to the sensor. As the focused ultrasound impinges upon a thermocouple, the thermocouple experiences a rapid increase in temperature due to the absorption of ultrasound in the thermocouple sheathing material and in the surrounding tissues. The multi-point search program measures the magnitude of the rising edge transient temperature of each sensor during each ultrasound burst. The transient temperature is measured by taking the difference in temperature measured before and after a 0.2 s ultrasound burst. An impulse of ultrasound at significant power is sent at every search step of the gantry position. The sonication power must be sufficient to cause a transient temperature greater than 0.2°C at the sensor location over a 0.2 s duration. This lower limit is used to eliminate any signals less than 0.2 °C occurring during the search which may be due to noise (to be discussed in Section 4.9). The closer the pulsed ultrasound focus is to the sensor, the higher the transient temperature measured by the sensor. Thus, the maximum transient temperature of this measurement is identified as the best known location of the sensor during the search. (The differences in transient effects on different thermocouple types are discussed in [5]).

4.3 Locate operation

A timing diagram of the ultrasound burst and temperature measurement is shown in Figure 4.2. At each point in the search grid, the temperatures on all probes are measured prior to the application of the ultrasound burst. The ultrasound is then turned on for a period of between 0.2 s and 0.4 s. The temperatures are measured prior to the end of the ultrasound burst beginning after the first 0.2 s of ultrasound. As mentioned in Chapter 2, the PC requires 0.2 s to complete a single read for all 16 probes (112 sensors). Thus, the ultrasound burst can last for 0.2 s to 0.4 s depending on the total number of probes being searched. The sensor with the maximum transient temperature at any given search step will be noted. This value is then compared with the old maximum transient temperature of the sensor. If this new transient temperature is larger then the old value, it means that power was deposited nearer to the sensor at this new location. Thus, the new location is closer to the sensor's physical location and the new transient temperature and gantry positions are updated for the respective sensor. If the new transient temperature is smaller than that of the old value, the new location is farther away from the old location and the new reading is discarded. The data format for storing the record of each sensor position and maximum transient temperature consists of the following series of 2D arrays:

(1) max(probe #,sensor #): maximum transient temperature of a sensor;

(2) xpos(probe #,sensor #): x gantry position of a sensor during the maximum transient;

(3) ypos(probe #,sensor #): y gantry position of a sensor during the maximum transient; and

(4) zpos(probe #,sensor #): z gantry position of a sensor during the maximum transient.

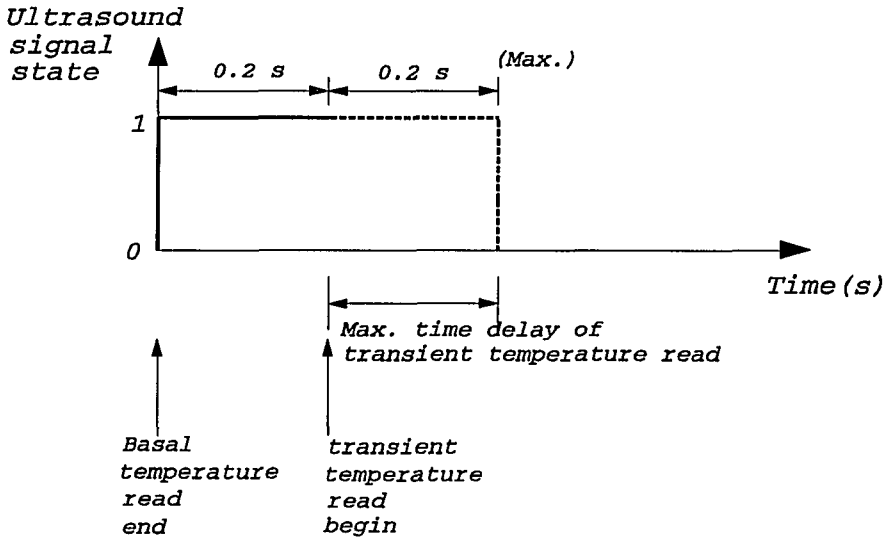

Figure 4.2 Timing diagram of locate temperature read

After each measurement and comparison of the transient temperature, the PC sends a command through the serial bus to the motion controller to move the gantry to the next position and repeats the measurements at the new location. The search routine will repeat this procedure until the entire search area is completed. The location

obtained by this search gives knowledge of the physical location of all sensors within the given search area.

4.4 Search path

The search pattern for the gantry movement is a rectangular raster scan (see Figure 4.3). The routine assumes the gantry is initially located in the center of the area to be searched. The operator then enters the desired x and y dimensions of the grid to search. The routine starts by moving to the -x, -y corner of the raster. The gantry is first stepped through the positive x direction until the x search limit is reached. The gantry is then incremented in the y direction and returned to the starting x position to continue the next scan line along x. This scan pattern will repeat until the y search size is reached. After the search area is covered, the gantry is returned to the negative x and y starting corner. If the z direction is to be searched, the gantry is incremented in the z direction and the search area repeated as before until the z search size is reached. At the end of each search, the gantry is moved back to its negative x, y and z starting corner. If the search area is completed or if the operator interrupts the search routine, the gantry will be brought back to the scan center again after it exits from the search routine. This particular search pattern is better than a continuous zigzag pattern because returning the gantry to the x start location on each increment in the y direction can avoid unknowns in position due to sloppy gears and chains along the x axis.

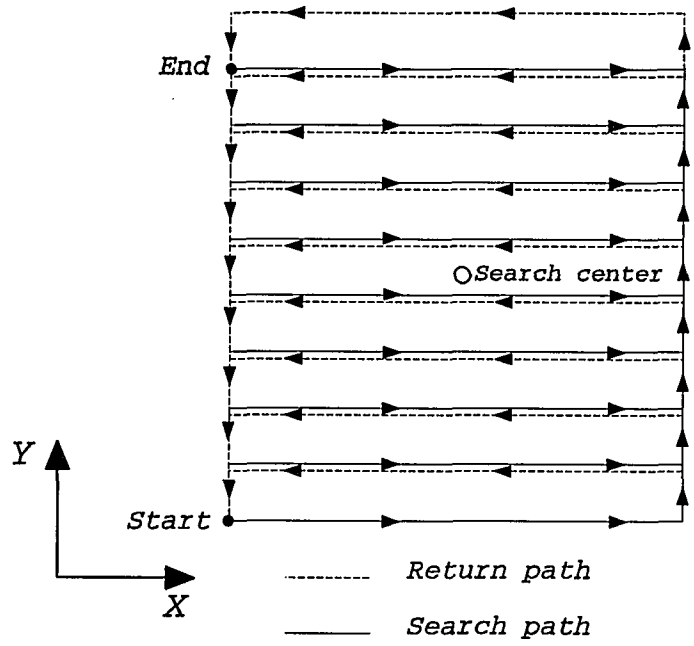

Figure 4.3 Search path

4.5 Flow chart of locate routine

A flow chart of the locate routine is depicted in Figure 4.4.

4.6 Experimental results of locate routine

An experiment was performed to test the multi-sensor search routine. The experiment used four polyethylene probes (with a total of 23 working sensors) implanted in an agar phantom, and a single transducer of diameter 70 mm and a radius of curvature equal to 250 mm operating at 1 MHz with an applied power of 18 W. The simulated focal point characteristic of this transducer in water is shown in Figure 4.5. Each contour line is a 10% step decrease of the relative ultrasound power from the inner rim to the outer rim where the center of the inner rim is given at 100% relative ultrasound power.

The setup for the physical position measurement of the sensors under search is shown in Figure 4.6. The x and y positions of each sensor were measured relative to the 3rd quadrant corner of the agar phantom to the nearest millimeter (by a 1 mm accuracy ruler) before placing the agar phantom on top of the ultrasound tank. This 3rd quadrant corner was marked by the intersection of two perpendicular threads running along edges of the agar phantom after placing the phantom on the ultrasound tank. The gantry was then positioned at the reference point and the position of the

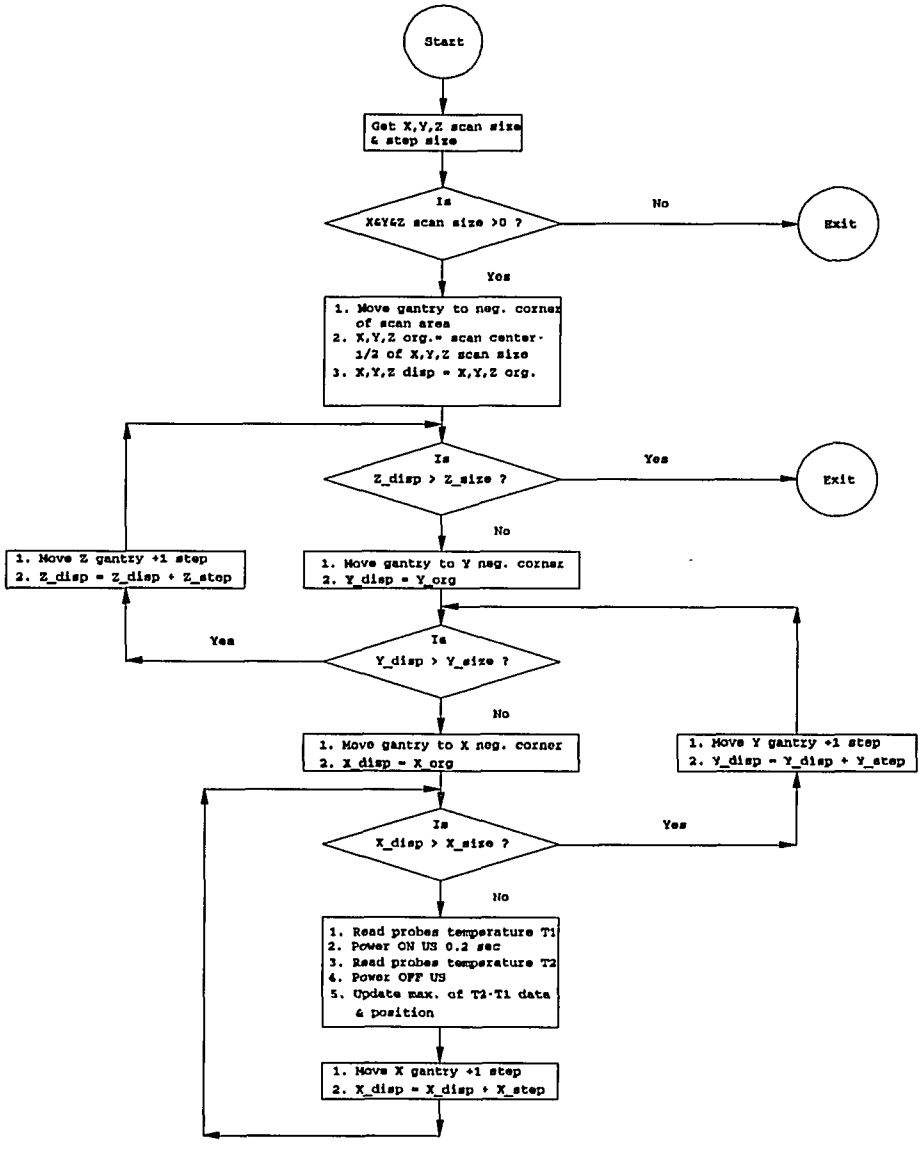

Figure 4.4 Flow chart of locate routine

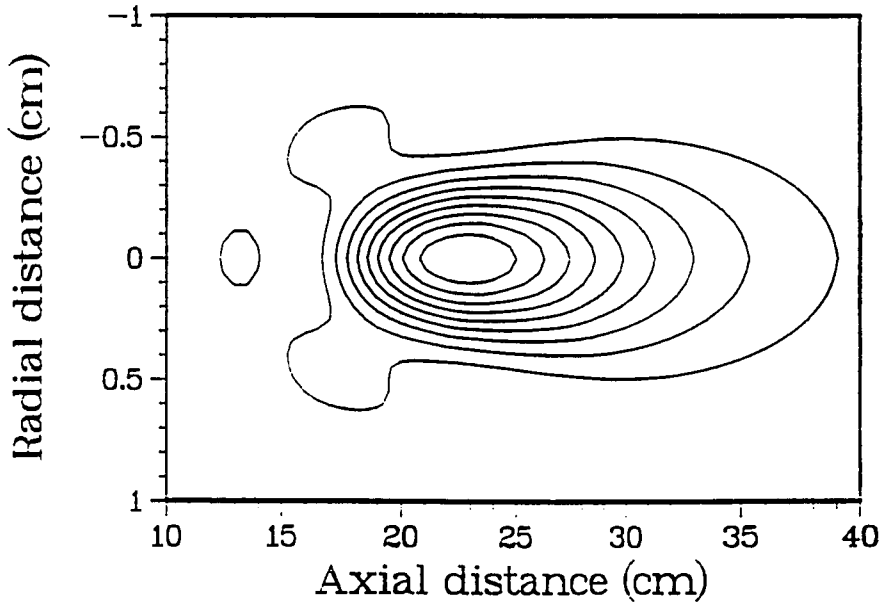

Figure 4.5 Ultrasound intensity plot of transducer

gantry was recorded. Thus, the reference position for the sensors was marked and the physical location of each sensor under search was calculated relative to the gantry position.

In the experiment, the gantry was first brought to its reset position where all axes assume their lowest possible limit positions. The gantry was then moved to the start position of the area to be searched. This was performed before every set of locate data was collected to ensure the multi-sensor search routine was repeatable following every gantry positional reset. Ten sets of data were collected using a scan area of

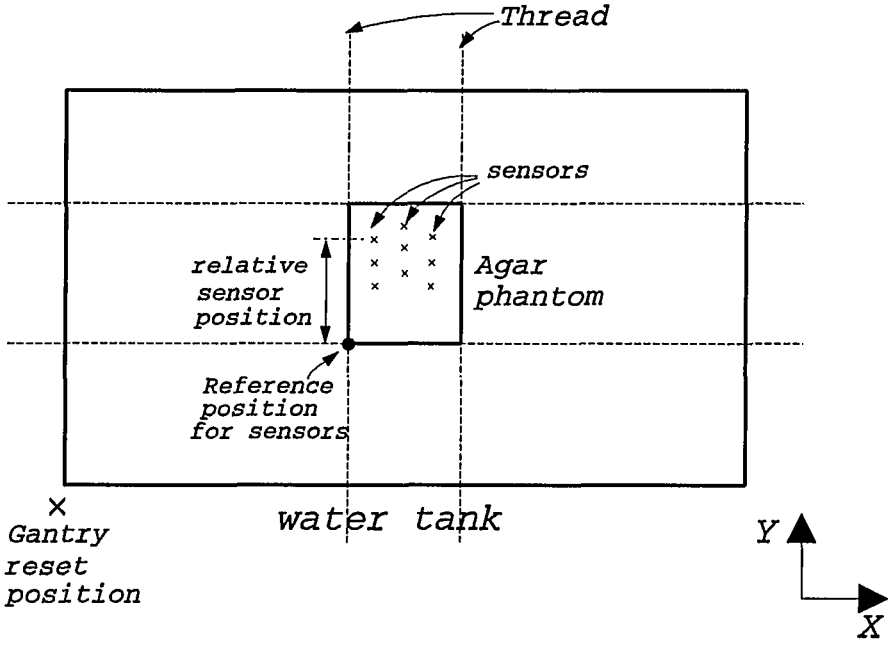

Figure 4.6 Setup for locate experiment

65mm (x) by 80 mm (y) using a 1 mm step size. Table 4.3 shows the results obtained from the experiments, where

Avg. error = Avg. locate data - measured position using a ruler.

The values obtained are within the limits of the physical measurements obtained with a 1 mm accurate ruler and the reinitialization procedure [4]. The average standard deviation of the error in the x direction was 0.609 mm and 0.384 mm in the y direction. This accuracy shows the consistency of the multi-sensor locate routine. The differences in standard deviation between the x and y axis can be analyzed using the following three factors: (1) arbitrary positioning of the sensors with a search step size

Sensors	X (mm)		Y (mm)	
	Avg. error	SDV	Avg. error	SDV
1	-0.5	1.41	+0.33	1
2	-0.2	0.97	-0.2	0.44
3	-0.1	0.93	-0.1	0.33
4	-0.1	0.78	0	0.5
5	-0.25	0.71	-0.28	0.44
6	-0.5	0.97	0	0
7	0	0.67	0	0
8	-0.1	0.56	0	0
9	+0.3	0.48	0	0
10	+0.3	0.42	-0.1	0.52
11	+0.8	0.79	+0.1	0.52
12	-0.3	0.42	+0.1	0.32
13	-0.2	0.63	0	0
14	0	0.53	+0.2	0.48
15	+0.1	0.32	-0.2	0.42
16	+0.1	0.57	-0.2	0.42
17	0	0.53	-0.5	0.707
18	-0.1	0.57	-0.2	0.48
19	-0.1	0.32	-0.1	0.32
20	-0.1	0.52	+0.1	0.52
21	+0.2	0.48	-0.1	0.52
22	0	0	+0.1	0.57
23	-0.2	0.42	+0.1	0.32
Total AVG:	-0.041	0.609	-0.041	0.384

Table 4.3 Locating system accuracy (mm) data for 10 repeated searches

of 1 mm, (2) sloppy mechanism in the x direction relative to the mechanism in the y direction, (3) the cool down time artifact (the system needs 3 s to cool down) [5]; the current search step absorbed heat from previous search steps along the x axis causing a reduction in the measured temperature rise along the x direction. The last factor could potentially explain the difference between the x and the y axis standard deviation, since the search in the y direction had a longer cool down time relative to the x direction.

4.7 Comparison of multi-sensor vs. single sensor search

The main difference between the new multi-sensor routine and the single-sensor locate routine, used previously, is that the multi-sensor locating routine requires less time to complete a search for the same area. Time can be saved with the multi-sensor locate routine because it searches for all of the sensors in a given area while the single sensor locate routine could only do as it's name implies - search for only one sensor in a given area.

Figure 4.7 shows the difference in procedure for the multi-sensor and the single sensor locating routines during a search for a particular sensor. When using the single sensor locate routine to search for the first sensor, if the sensor is not found a new guess must be made regarding the best direction to move for the next search area. This can be very time consuming since at least two or more search executions are needed.

In contrast, even if the multi-point sensor search may not find the particular sensor in the current search area, a group of sensors will be found under the current search area. From the information obtained from this group of sensors, the move to the next search area to find a particular sensor is made easier.

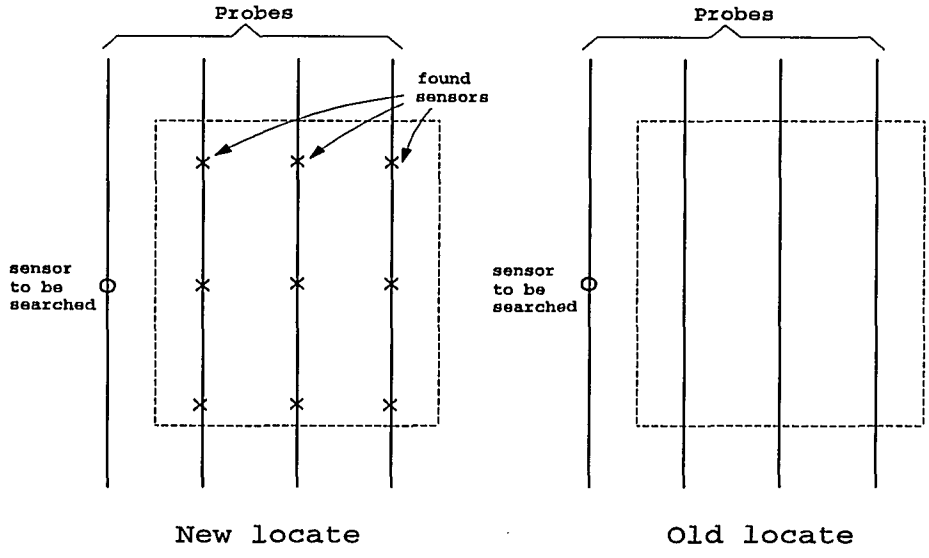

Figure 4.7 Multi-sensor search and single sensor search

Another case for comparison of the two search routines is when n sensors are to be located. The multi-sensor locate routine only needs one execution to locate the n sensors, whereas, n searches are needed by the single-sensor routine. Besides, the operator needs to partition each sensor search area for the single-sensor search such that one sensor can be found at a time. If the partition is overlapping, as shown in Figure

4.8 (which is usually the case due to the short distance between sensors, 10 mm apart), the search time during n overlapping searches is wasted. Thus, time can be saved by using the multi-sensor search because no overlapping of the search area exists.

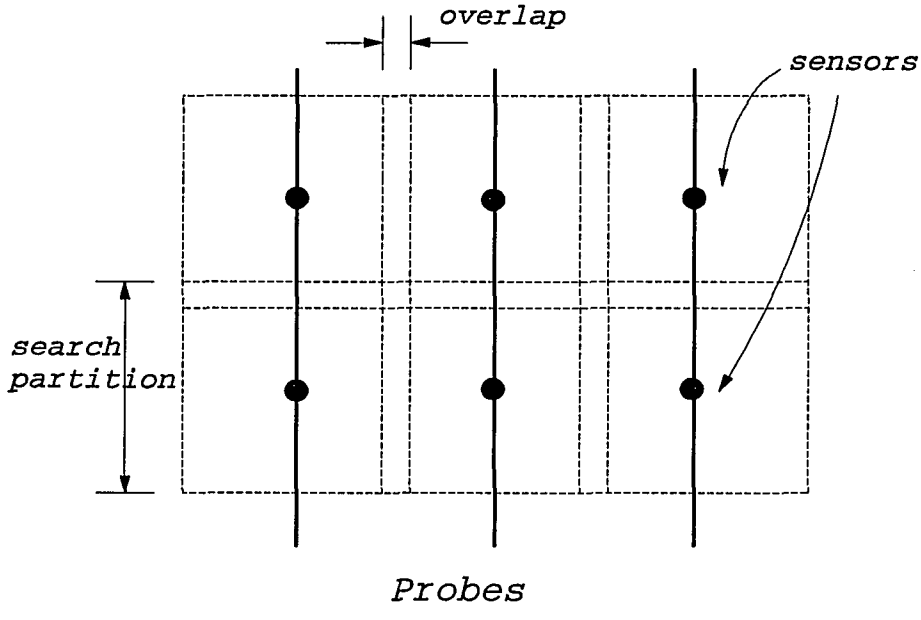

Figure 4.8 Single sensor search overlap

4.8 Problems in the multi-sensor search

Although the multi-sensor locate routine has advantages over the single-sensor locate routine, there are problems that the multi-sensor locate routine could not overcome. These problems are discussed below.

4.8.1 Out of boundary

Sensors which lie outside the search area may be indicated as found by this search routine if the sensor is located close to the search boundary as in Figure 4.9. This location is not the true sensor position but rather the operator's best knowledge of the sensor's physical location. Thus, the sensor positions located by this routine are reliable only when the sensor is lying within the search area.

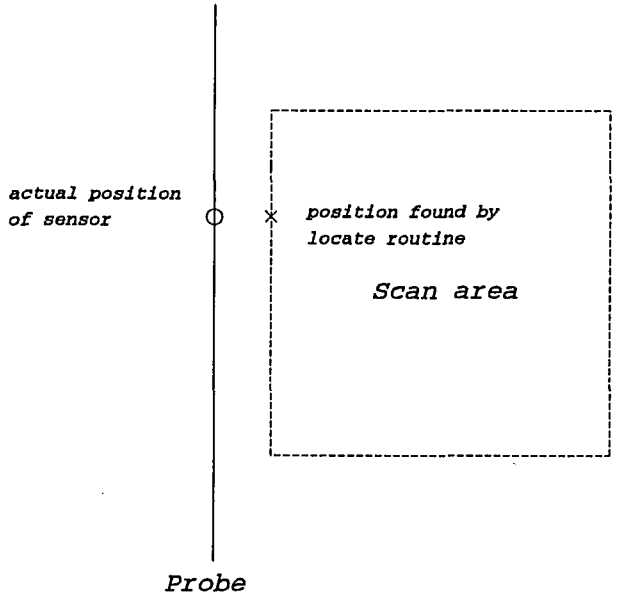

Figure 4.9 Out of boundary search

4.8.2 The diameter of the focus

The sensor location indicated as found by the search may not be exact even though the sensor lies within the search area. If the focus diameter of the transducer is large and blunt, the maximum transient temperature read while pulsing the ultrasound is not confined to a specific point as in Figure 4.10. If 1 mm steps are used with a 5 mm diameter and blunt focus, large transients may be indicated up to 5 times. Thus, an inaccurate location could be obtained with transducers having a large diameter focal region.

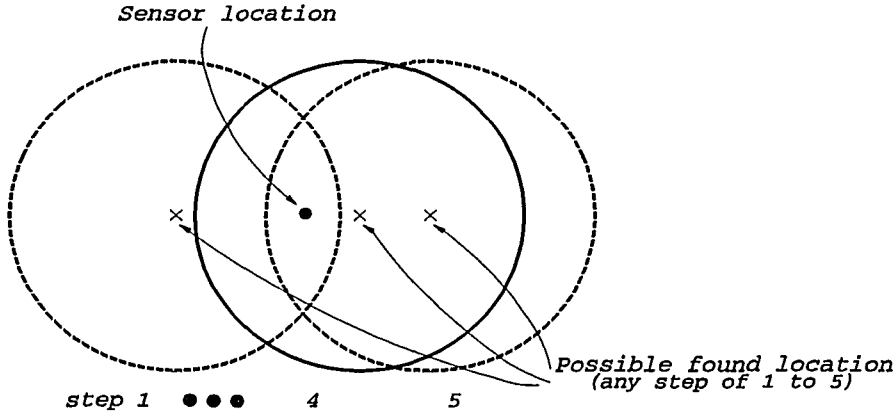

Large diameter focus

Figure 4.10 Large focus diameter transducer

4.8.3 Depth of the focus

If the depth of the focus is not in the plane of the sensors to be found, the results may suffer the same effects or even larger, as those for a transducer with a large and blunt focus diameter. The location indicated as found could be inaccurate as in Figure 4.11.

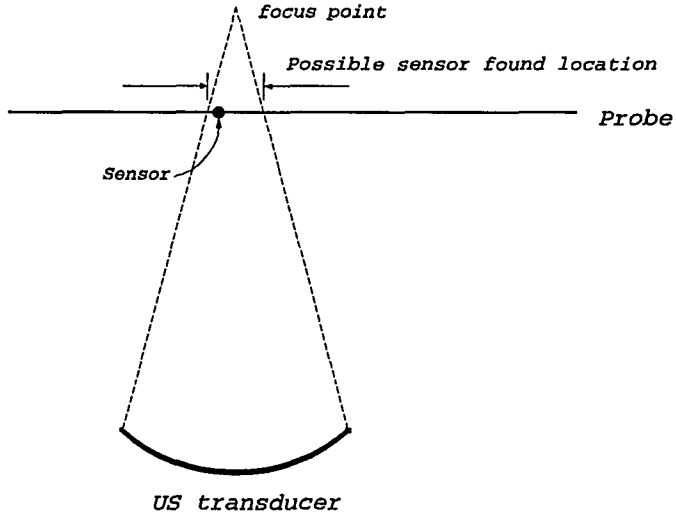

Figure 4.11 Out of focus depth

4.8.4 Search resolution

The search resolution could cause an inaccurate reading during a search as shown in Figure 4.12. This error is because if the search step is x mm, then the best search error is ± x/2 mm. The accuracy of a search is approximately half of the actual search step size if all the other search factors above are assumed to be accurate.

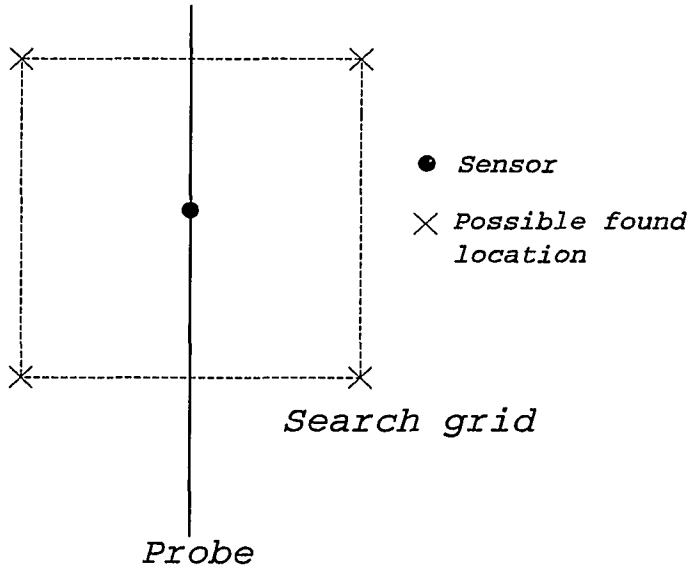

Figure 4.12 Large search resolution

4.8.5 Reflections

The reflection problem is a more difficult problem than the above four. This situation can be due to air bubbles or a rough surface interface in the direction of the ultrasound signal that causes a redirection of the beam. Bone and air have acoustic impedances which are very different from those of soft tissue. Because of this acoustic difference, a significant amount of ultrasound energy is reflected at soft tissue/bone and soft tissue/air interfaces. In addition, refocussing may occur if these interfaces are curved. These reflections follow the basic principles of optics. The sensor may absorb more power than it should be during an impulse of ultrasound due to the additional power reflected from nearby non absorptive material as in Figure 4.13 and Figure 4.14. With this condition, the search strategy will not perform effectively and imaging techniques like CT may be necessary to help plan the treatments.

4.9 Noise rejection

Noise during location searches can cause false sensor positions to be indicated. This can be due to electrical noise while sending an ultrasound burst and trying to read the temperature at the same time. A noise rejection factor is added into the multi-sensor locate routine such that any transient temperature lower than this factor will be rejected (not considered as a potentially found sensor). If this factor is too high, the

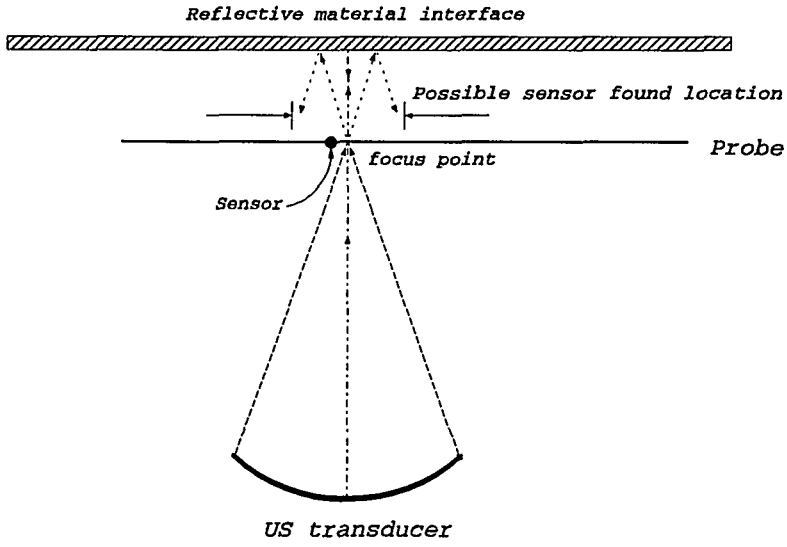

Figure 4.13 Reflective material (flat)

sensor can not be found, and if it is too low then many false locations are found. During development of this locating system, it was found that 0.2 °C can provide a reasonable noise rejection during the multi-sensor search routine at a power of 13 W with polyethylene probes and 0 mm depth penetration for the agar phantom. The noise rejection factor not only helps filter out the noise caused from the two above sources, but it also helps to correct the location problems discussed in Section 4.8 to a certain extent. However, the noise rejection factor is fixed at 0.2 °C in this locating system during treatments. The operator is required to adjust the ultrasound power bases on the nature of the treatment to perform a safe and effective location search for the sensors.

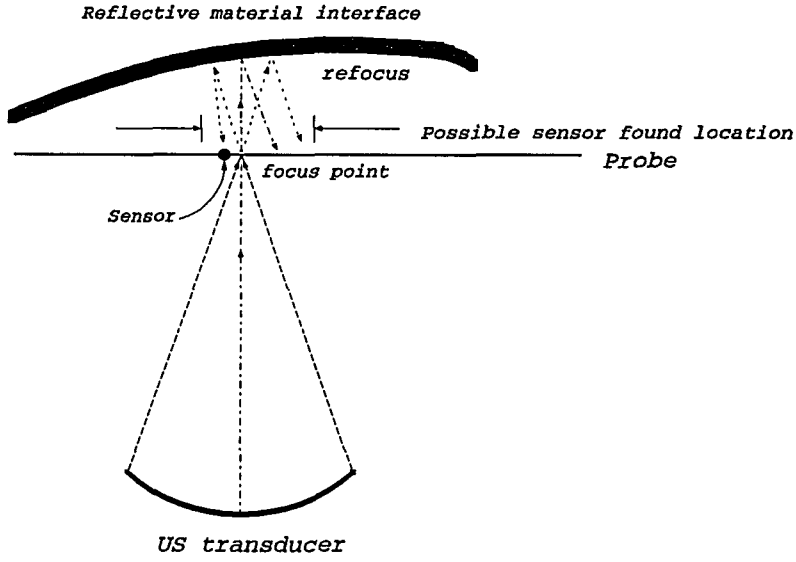

Figure 4.14 Reflective material (curved)

In addition to the noise rejection factor, the operator at any time may still need to confirm the location found by this search routine by comparing the sensor's location and the transient temperatures to that of a neighboring sensor to ensure that the correct sensor location is found.

CHAPTER 5

DISCUSSION, CONCLUSIONS AND SUGGESTIONS FOR FUTURE WORK

In this study, a new thermometry system for use in ultrasound hyperthermia has been developed. A complete reading with temperature conversion before display for 112 thermocouple sensors (16 probes) takes only 0.2 s. This is a significant increase in reading speed compared to that of the old thermometry system. An average accuracy of ± 0.05 °C under normal operation conditions (ambient temperature 22 °C to 28 °C) was achieved. A probe to earth ground leakage sink current of 75 μA and a leakage source current of less than 10 μA was attained. Although the new system hardware does not meet the medical safety aspect of leakage sink current to earth ground when bare probes are used, this could be easily corrected by inserting a DC-DC isolation power supply into the system DC supply path at the opto-isolation unit and by moving the opto-isolation unit as close to the TAU as possible (see Appendix C).

The multi-sensor locate routine of a 2D x and y direction search was found to be reliable and effective. However, the location of the z plane in which to do the search is still enormously dependent on the ultrasound imager which provides the

operator adequate depth information. Overcoming the limitations of searching in the z direction, as discussed in Section 4.8 could be the subject of a future development for this thermometry system. Also, an intelligence search to detect and solve the out of boundary problem is of interest for future work. The out of boundary problem can be detected by noticing the found location which lie on the boundary. This search may then automatically pursue the location by searching the nearby area outside the boundary until the location is found.

Two main technical recommendations for future manufacturing of an ultrasound hyperthermia thermometry system are suggested as, one, the reduction in equipment temperature drift and, two, the efficiency of electrical isolation. The equipment temperature drift can be reduced by two main factors which are the temperature difference of the connector and the temperature coefficient of the instrumentation amplifier. The temperature difference of the connector can be reduced by enclosing the entire connector inside a thermal insulator or by an isothermal block such that the temperature difference of the connector can be reduced. Indeed, if the internal thermocouple wire can be eliminated then the temperature difference of the connector is eliminated. The temperature drift of the amplifier can be reduced by using a lower temperature drift coefficient instrumentation amplifier and by having a stable environmental temperature for the amplifiers. The environmental temperature variations can be reduced by lowering the overall component power consumption of the TAU by choosing low power components such that the components heating effect can

be reduced. In addition, a thermally insulated enclosure will be a better approach than a metal (currently is aluminum) enclosure such that drastical external temperature change will not affect the internal temperature of the enclosure. This thermal insulation technique for the TAU enclosure will help to sustain a stable internal environmental temperature for a more stable thermometry system.

A recommendation for improving the electrical isolation is to move the opto-isolation unit as close to the TAU as possible such that leakage sink current can be efficiently reduced to the DC-DC isolation power supply product's leakage current specification. If the opto-isolation unit has to be contained within the same enclosure with the TAU, then a thermal insulation partition should be setup to separate the enclosure into two compartments such that heat generated by the optical-isolation unit which has high heat generation will not affect the TAU compartment's temperature. The insulation partition will help to provide thermally stable temperature measurements while the opto-isolation unit provides efficient electrical isolation.

A closer analysis of lowering the leakage sink current for this isolated thermometry system has been carried out. For a maximum allowable (UL544 specification) leakage sink current of 20 μA at 110 V 60 Hz AC, the minimum impedance or maximum capacitance is 5.5 MΩ or 482.28 pF, respectively. In order to meet the medical isolation specifications: (a) the leakage current from long isolated power lines parallel to earth ground cabling has to be reduced, and (b) a DC-DC isolation power supply which provides very low leakage current to earth ground must

be inserted after the AC-DC medical grade power supply. The dielectric constant of a cable is approximately 4 or higher resulting in a capacitance of 600 pf over a 4 m long cable. One way to solve this problem is to have an insulated enclosure for the front stage such that the earth ground conductor from the opto-isolation unit to the TAU can be eliminated. Thus, there would not be a long ground line running in parallel with the isolated DC power line and signal lines. Another solution is to move the isolation unit to the front stage within the TAU such that leakage through cabling is eliminated. The latter suggestion will increase the size and the heat generation of the front stage, since the isolated power supply and the opto-isolator are high heat generating components and is not a preferred alternative in a thermometry system design. Thus, an insulated enclosure will be a better approach. Inserting A DC-DC isolation power supply after the current AC-DC power supply in this thermometry system will provide sufficient isolation for the leakage sink current of the equipment [21].

Besides the above technical discussion, from clinical considerations, the overall system size should be as small as possible. A small size would make the system more portable and capable of being placed as close to the patient as possible during treatment in order to reach the patient in any position with a minimum thermocouple length. The size of the current TAU is 43 x 30 x 31 cm^3 (length x depth x height) which is considered large during application.

In response to the above technical recommendations and the size constraint of the thermometry system, a second version of the thermometry system is being

developed. The technical details of the second version TAU will be in Appendix C.

APPENDIX A

THERMOMETRY SYSTEM I SCHEMATIC

APPENDIX A.1 Bus driver buffer schematic

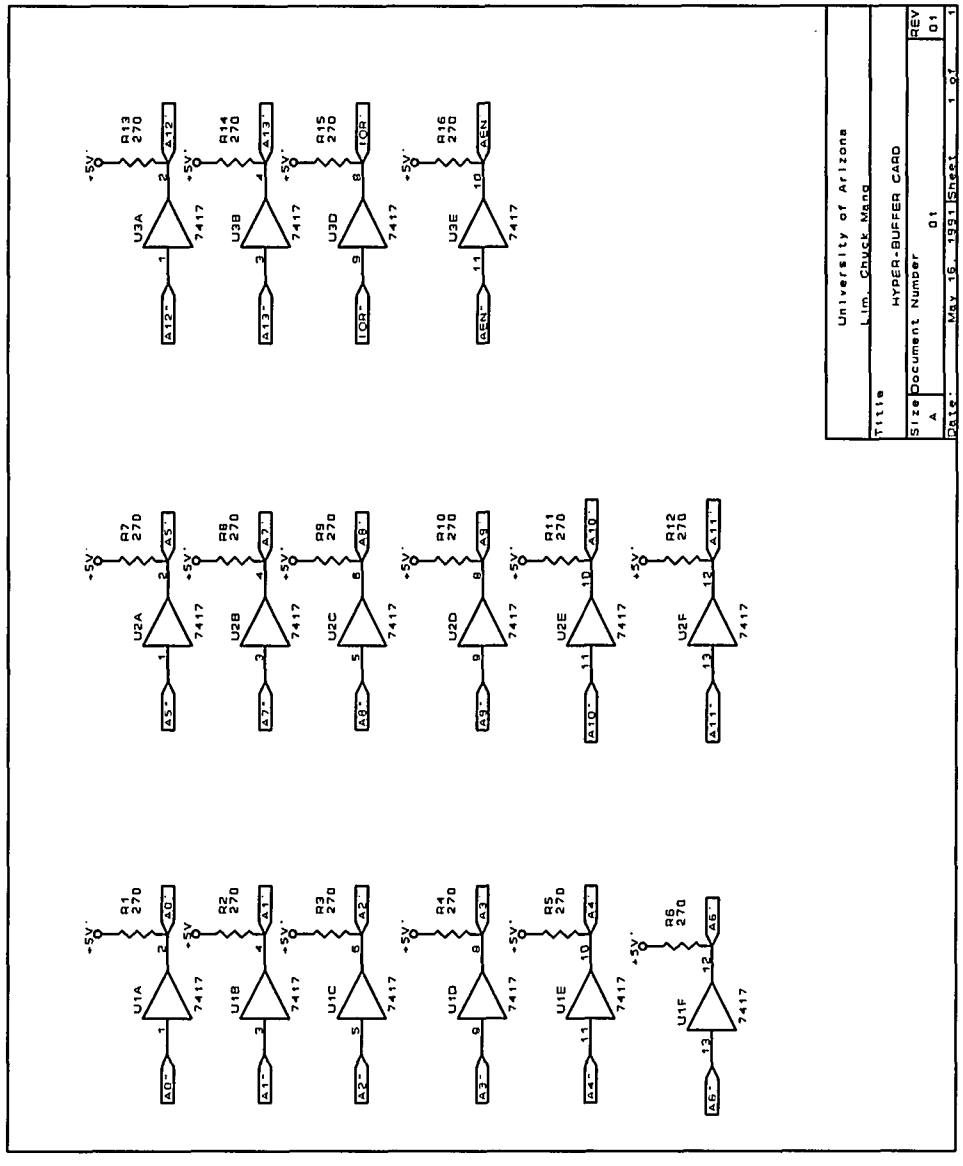

APPENDIX A.2 Opto-isolation unit schematic

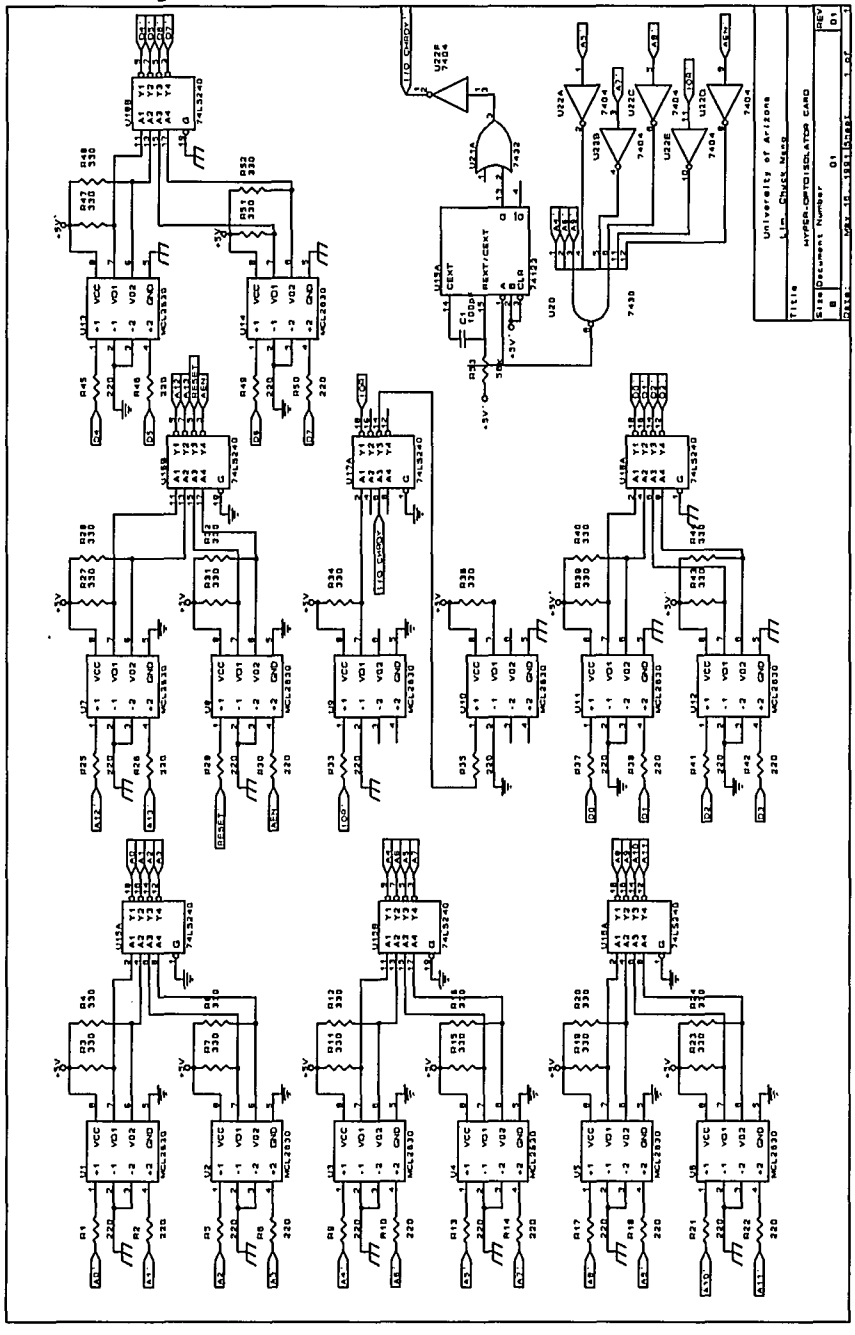

APPENDIX A.3 Card select and pulsing card schematic

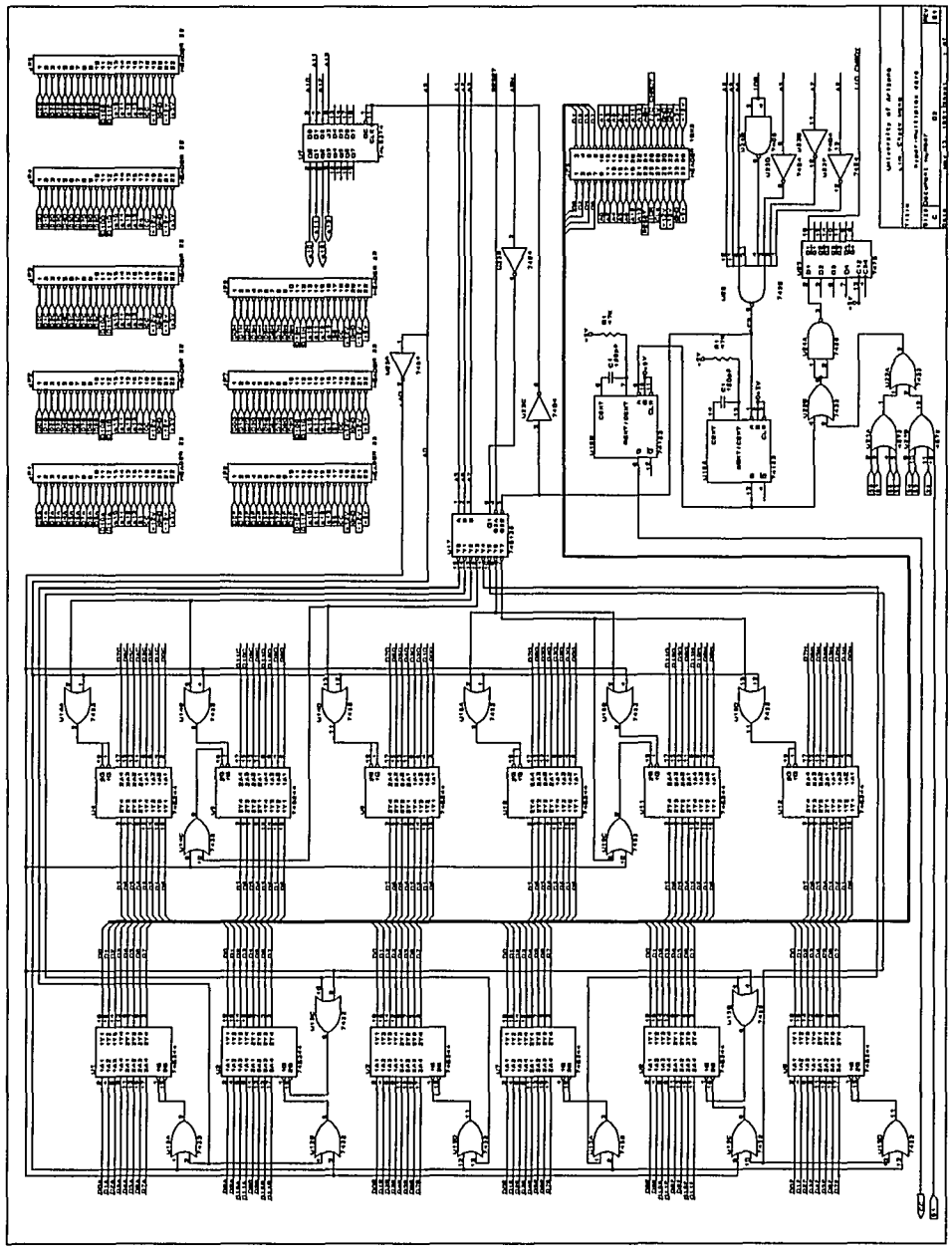

APPENDIX A.4 Amplifier card schematic

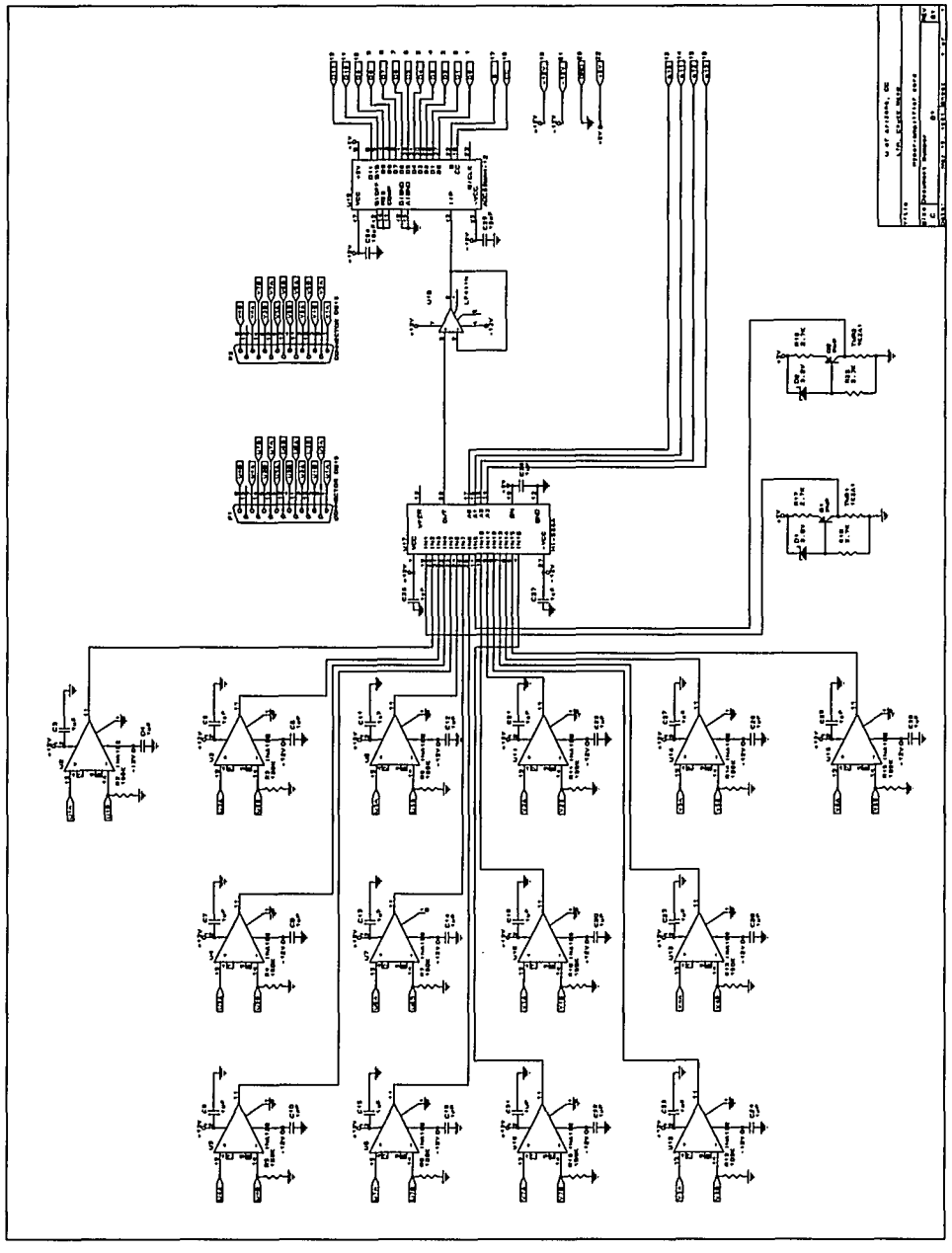

APPENDIX B

THERMISTOR DATA

Thermistor	I (mA)	A	B	C
1	7.187597e-4	1.418867e-3	2.669310e-4	2.700016e-7
2	7.291344e-4	1.298141e-3	2.9311444e-4	8.754092e-8
3	7.037028e-4	1.394124e-3	2.719831e-4	2.387166e-7
4	7.320608e-4	1.366126e-3	2.781344e-4	1.967668e-7
5	7.170030e-4	1.450476e-3	2.597500e-4	3.216794e-7
6	7.246132e-4	1.383428e-3	2.744192e-4	2.214919e-7
7	7.607862e-4	1.472134e-3	2.553828e-4	3.522415e-7
8	7.020155e-4	1.434652e-3	2.629288e-4	3.073780e-7
9	7.232435e-4	1.458833e-3	2.579354e-4	3.389484e-7
10	7.013178e-4	1.423369e-3	2.657241e-4	2.810323e-7
11	7.300442e-4	1.440610e-3	2.619063e-4	3.097808e-7
12	7.240200e-4	1.352155e-3	2.815775e-4	1.691701e-7
13	7.288759e-4	1.452974e-3	2.589610e-4	3.267778e-7
14	7.653114e-4	1.652015e-3	2.160272e-4	6.260866e-7
15	7.181200e-4	1.298589e-3	2.930799e-4	8.709648e-8
16	7.287870e-4	1.360774e-3	2.789226e-4	1.863583e-7

$$T = 1/(A + B \ln(R) + C (\ln(R))^3$$

where,

T: temperature (degree Kelvin)
R: resistance of thermistor
A, B, C: curve-fitting constants

Table B Thermistor current and coefficient

APPENDIX C

VERSION 2 TAU

Version 2 TAU is an improved thermometry system over the 1st because it will have a lower equipment temperature coefficient, a lower leakage sink current, and a smaller overall size. The main hardware differences from the 1st version are

(1) combining the opto-isolation unit with the TAU enclosure, as shown in Figure C.1, in order to reduce the leakage current by eliminating the long cabling that picks up leakage current (Figure 2.1),

(2) enclosing the connector within the isothermal block and eliminating the internal thermocouple wire will eliminate the temperature difference across the connector pin, as shown in Figure C.2,

(3) placing an isothermal plate (aluminum) in contact with all instrumentation amplifiers on the same card to obtain lower temperature differences between amplifiers, as shown in Figure C.2,

(4) inserting a DC-DC isolation power supply (CALEX, 12D5-12SW) whose leakage current is approximately 9 μA to provide low leakage current isolation power supply to the front end, as shown in Figure C.4,

(5) replacing the A/D converter by a lower power A/D converter (MIXIM, MAX167ACNG) with a built in tri-state buffer for lower heat generation,

(6) replacing the instrumentation amplifier INA102KP by INA102CG which is a better

grade amplifier in terms of having a lower input offset drift temperature coefficient, and (7) re-sizing of the PCB (printed circuit board) for a smaller size of the TAU.

This appendix will discuss detail changes made for the 2nd version TAU.

C.1 General modification

C.1.1 General structural modification

The opto-isolation unit has been included into the enclosure of the TAU as shown in Figure C.1 for more efficient electrical isolation. The DC-DC power supply and the opto-isolator are the two main heat generating components of the opto-isolation unit. Thus, a thermal partition is set up to isolate air flow from the opto-isolation unit, which generates heat, to the amplifier unit. The TAU is powered by a +12V DC supply while electrical isolation is performed within the TAU.

C.1.2 Amplifier layout modification

Two layout modifications are made on the amplifier card as shown in Figure C.2. First, the connector is relocated from the front panel to the amplifier card. The connector is then sandwiched between an isothermal block and the PCB. This relocation eliminates the effect of the temperature difference across the connector by eliminating the internal thermocouple wire and using a connector pin that has the same copper material as the copper track on the amplifier card (the connector pins are copper tinned with gold). However, the thermocouple probe's wire to the copper wire

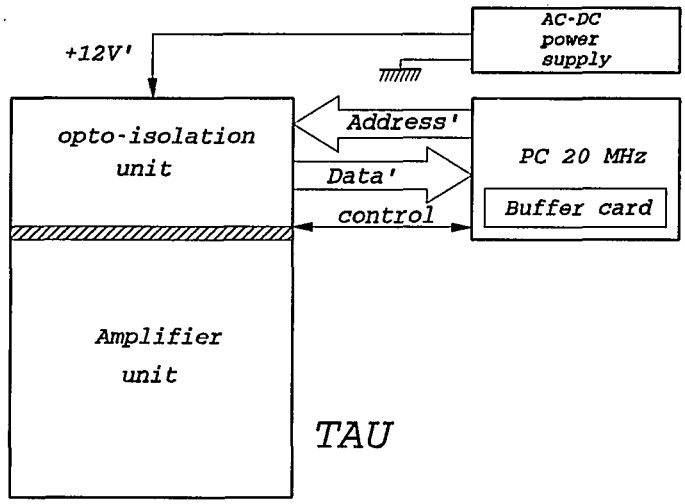

Figure C.1 Version 2 TAU block diagram

junctions do not make direct contact with the isothermal block. The reference junction temperature, which occurs on the patient's (probe's) connector, is estimated by the isothermal block temperature. This isothermal block is in direct contact with the copper track of the PCB located adjacent to the connector pin mounting on the amplifier card, such that any thermal change on the isothermal block can be transferred quickly to the reference junction. Thus, the temperature coefficient of the connector effect is reduced and the reference junction temperature is measured. Second, an isothermal plate which is in contact with all amplifiers on the amplifier card is added to reduce the temperature variation among the amplifiers on the same card.

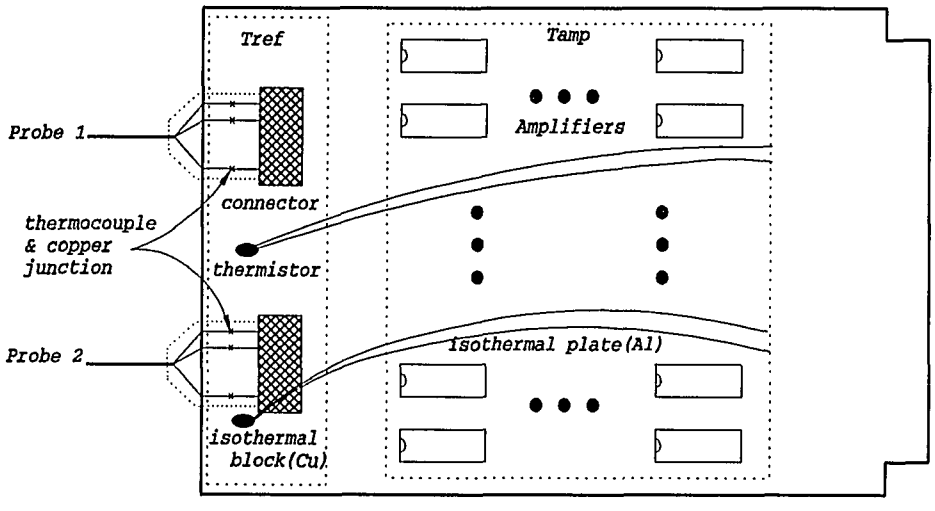

Figure C.2 Connector position on amplifier card

C.2 Electrical hardware modification

C.2.1 Buffer card modification

The main modification on the buffer card is relocation of the base address decoder from the card select and pulsing card to the buffer card such that only the base address is sent to the TAU, as shown in Figure C.3. This reduces the number of conductors running from the PC to the TAU and thus a smaller connector is required. Another change is using the 74HCT244 as a line driver instead of a 7414, for it's lower power consumption and so that no external resistor is required.

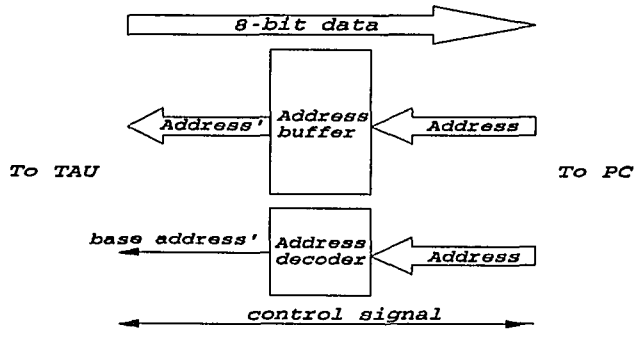

Figure C.3 Buffer card block diagram

C.2.2 Opto-isolation card modification

Many modifications were made on this card. The modifications mainly combine both the opto-isolation card with the card select and pulsing card of the 1st version into the opto-isolation card of the 2nd version, as shown in Figure C.4, for efficient space utilization and lower PCB manufacturing cost. In addition, the control logic for the new A/D converter has changed due to the difference between the old and the new A/D converter. Also, a DC-DC isolation power supply was added to provide isolated power to the front end components such that electrical isolation for the medical leakage sink current specifications can be satisfied.

On the non-isolated end, a 9 μs delay circuit is set up to hold the PC while the selected TAU is waiting for the thermocouple signal to settle through multiplexing and to get ready for the A/D conversion. The PC hold logic is used to combine the 9 μs delay signal and the return status from the A/D converter. A data buffer is used to drive the return data after the opto-isolator to the PC.

On the isolated end, a DC-DC isolation power supply (leakage current of 9 μA) is inserted after the AC-DC power supply such that leakage sink current is reduced to satisfy the UL544 leakage current specification when bare probes are used. Data buffers are used to buffer the data signals from the A/D converter to the opto-isolator. A clock logic is included in this version to provide 1 MHz clock pulses to the A/D converter which requires an external clock signal. The address latch & logic, together with the card multiplexer is used to select one sensor at a time from an amplifier card. Similar to the 1st version, the selected sensor's analog signal is then converted into digital signal and sent from the A/D converter to the data buffer on the isolation end.

C.2.3 Amplifier card modification

Three electrical modifications are made on this card, as shown in Figure C.5. First, the old instrumentation amplifier (INA102KP) is replaced by a better grade amplifier (INA102CG) in terms of input offset drift temperature coefficient. This improves the temperature stability over the normal operational range of the thermometry system. Second, the A/D converter is replaced by a 1/3 less power A/D converter with built in tri-state buffer. This reduces the overall power consumption and the heat generation of the TAU. This also provides a common data bus wiring on the amplifier card's edge connector such that the number of wires needed is reduced. Third, the unity gain buffer is not required by the new A/D converter, as specified by the manufacturer. Thus, fewer components were used and the power consumption was

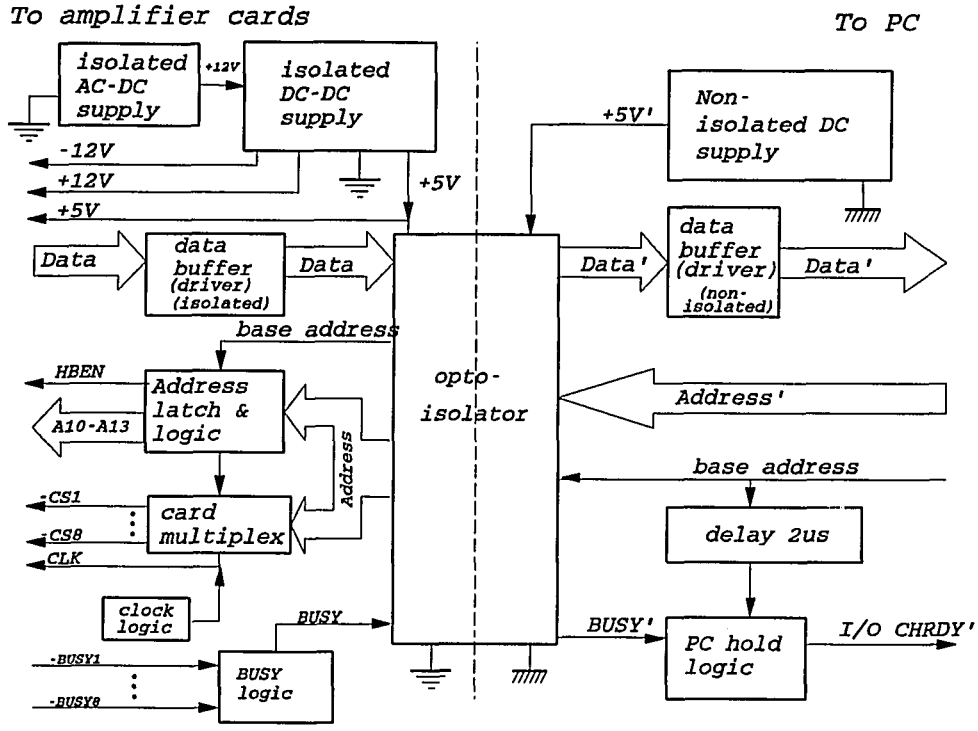

Figure C.4 Opto-isolation unit block diagram

further reduced.

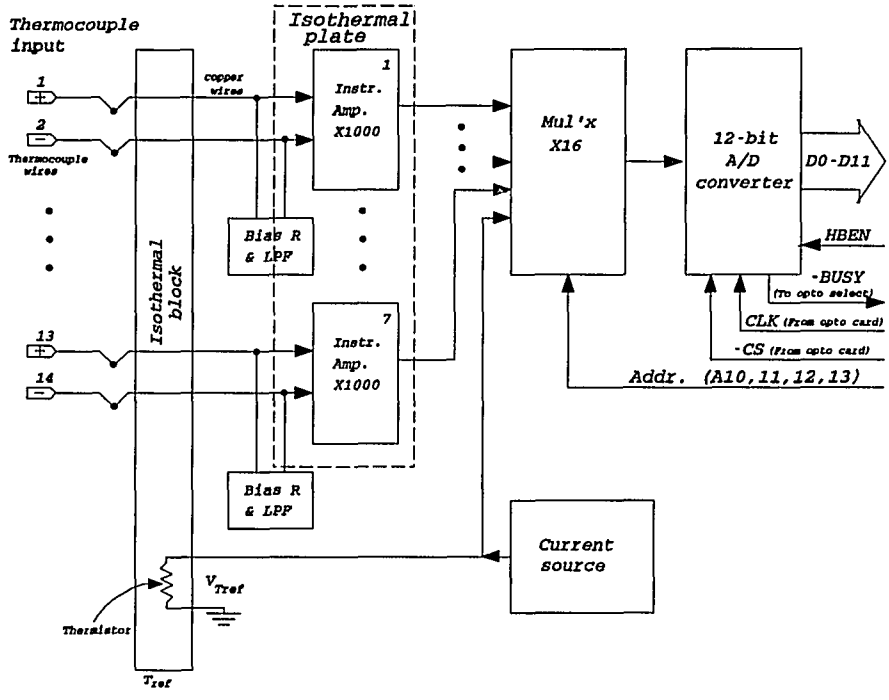

Figure C.5 Amplifier card block diagram

APPENDIX D

CONNECTORS

Two types of connector were used on the old thermometry system. One is a 14-pin 7 sensor connector and another is a 9-pin 7 sensor connector. However, only the 14-pin 7 sensor connector can be used on the new thermometry system. The equivalent circuit of the difference between the 14-pin and the 9-pin connector measured on the new thermometry system is shown in Figure D.1.

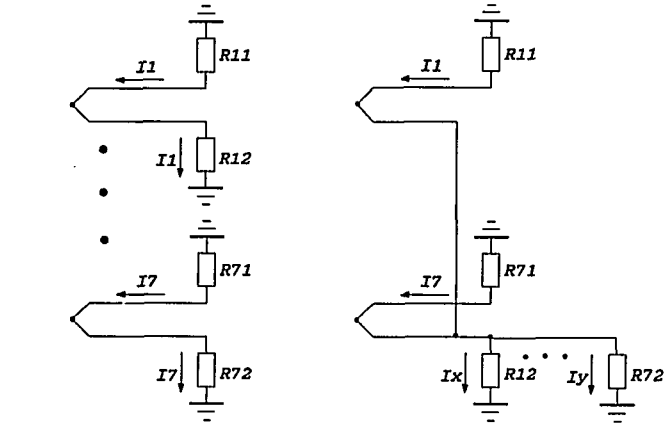

Figure D.1 Difference in connector

The 9-pin 7 sensor connector was able to be used on the old thermometry system because only one sensor was multiplexed and measured each time. The voltage read

by the volt meter was the actual value of the measured sensor. On the other hand, if the 9-pin 7 sensor connector were to be used on the new thermometry system which has a merge and then split connection at the connector pin, this would cause a different current flow in the negative terminal of the measurement point. Hence, the voltage measured would not be the sensor's actual voltage. Therefore, the 9-pin 7 sensor connector can not be used on the new system.

APPENDIX E

SYSTEM SOFTWARE

A menu oriented software package was written to provide the operator with a user friendly terminal during operation. All software were written in Microsoft quick basic language version 7.0. The entire system is window driven. There are a total of three main programs which coordinate the entire system operation: the main thermometry system package, the calibration package and the temperature viewing package. The thermometry system software package allows the user to re-initialize the gantry, edit treatment parameters, set the Wavetek function generator, select treatment temperature measurement and locate probes. Temperature measurement alone is also included as an option under the main software. This is to verify the thermocouple's are working prior to medicating the patient for treatment. The calibration package is to calibrate thermocouple probes using a two point calibration before the thermocouple probe is used. The temperature view package is for displaying a temperature vs. time graph at any time following treatment for any desire range of temperature and time period to better scrutinize the treatment temperature progress. Refer details operation of this system to the "Operator user manual for TAU" [28].

REFERENCES

[1] Lele, P.P., "Hyperthermia by ultrasound," Proceedings on the International Symposium on Cancer Therapy by Hyperthermia and Radiation, pp. 168-178, Washington D.C., 1975.

[2] Hynyen, K., "Biophysics and technology of ultrasound hyperthermia," Reprint from Clinical Thermology, Subseries Thermotherapy, Methods of External Hyperthermic Heating, Copyright, Springer Verlag, Berlin, Heidelberg, 1990.

[3] Anhalt, D., "Modification of a diagnostic ultrasound units movement system to perform scanning during focussed, ultrasound hyperthermia," Master's Thesis, University of Arizona, 1986.

[4] Kudrimoti, A.S., "Design and implementation of gantry movement controller and simple scanning patterns in ultrasound hyperthermia," Master's Thesis, University of Arizona, 1990.

[5] Hynynen, K., and Edwards, D., "Temperature measurements during ultrasound hyperthermia," Medical Physics, Vol. 16, No. 4, pp. 618-626, 1989.

[6] Fry, W.J., and Fry, R.B., "Determination of absolute sound levels and acoustic absorption coefficients by thermocouple probes-theory," Acoustical Society of America Journal, Vol. 26, pp. 294-310, 1954a.

[7] Fry, W.J., and Fry, R.B., "Determination of absolute sound levels and acoustic absorption coefficients by thermocouple probes-experiments," Acoustical Society of America Journal, Vol. 26, pp. 311-317, 1954b.

[8] Hynynen, K., Martin, C.J., Watmough, D.J., and Mallard, J.R., "Errors in temperature measurement by thermocouple probes during ultrasound induced hyperthermia," British Journal of Radiology, Vol. 56, pp. 968-970, 1983.

[9] Fessenden, P., Lee, E.R., and Samulski, T.V., "Direct temperature measurement," Cancer Research (Suppl.), Vol. 44, pp. 4799-4804, 1984.

[10] Wickersheim, K.A., Sun, M.H., and Samulski, T.V., "Ultrasound-immune fiberoptic thermometry probe," in Proceedings of the 33rd Annual Meeting of Radiation Research Society, Los Angeles, CA, pp. 61-62, 1985.

[11] Hynynen, K., Roemer, R., Anhalt, D., Johnson, C. Xu, Z.X., Swindell, W., and Cetas, T., "A scanned, focused, multiple transducer ultrasonic system for localized hyperthermia treatments," International Journal of Hyperthermia, Vol. 3, pp. 21-35, 1987.

[12] Hynynen, K., and Lulu, B.A., "State of the art in medical hyperthermia in cancer treatment," Investigative Radiology, Vol. 25, No. 7, pp. 824-834, July 1990.

[13] Hynynen, K., Shimm, D., Anhalt, D., Stea, B., Sykes, H., Cassady, J., and Roemer, R., "Temperature distributions during clinical scanned, focussed ultrasound hyperthermia treatments," International Journal of Hyperthermia, Vol. 6, pp. 891-908, 1990.

[14] Anhalt, D., and Hynynen, K., "Thermocouples - the Arizona experience with in-house manufactured probes," submitted International Journal of Hyperthermia, 1991.

[15] Kinzie, P.A., and Moore, R.D, "Thermocouple Temperature measurement," Wiley-Interscience Publication, 1973.

[16] Shambrook, K.P., "Signal processing techniques for temperature measurement," Temperature, Americans Institute of Physics, New York, Vol. 5, pp. 1167-1172, 1982.

[17] Reed, R.P., "Thermoelectric thermometry: A functional model," Temperature, Americans Institute of Physics, New York, Vol. 5, pp. 915-922, 1982.

[18] Underwriters Laboratories. Medical and Dental Equipment (UL544). Melville, NY: UL,1976

[19] National Fire Protection Association. Health care facilities (ANSI/NFPA 99-1987). Quincy, MA:NFPA, 1987.

[20] Association for the Advancement of Medical Instrumentation. Safe current limits for electromedical apparatus (ANSI/AAMI ESI-1985). Arlington, VA:AAMI, 1985.

[21] Ghahary, A. and Webster, J.G., "Electrical safety for an electrical impedance tomograph," IEEE engineering in Medicine & Biology Society 11th Annual International Conference, pp. 461-462, 1989.

[22] Shrivastava, P., Luk, K., Oleson, J., Dewhirst, M., Pajak, T., Paliwal, B., Perez, C., Sapareto, S., Saylor, T., Steeves, R., "Hyperthermia quality assurance guidelines," International Journal of Radiation Oncology Biology.Physics, Vol. 16, pp. 571-587, 1989.

[23] Lele, P.P., "Thresholds and mechanisms of ultrasonic damage to organized animal tissues," In Hazzard DG, Litz ML (eds) Symposium on biological effects and characterizations of ultrasound sources. DHEW publication FDA 78-8048. United States Department of Health, Education and Welfare, Rockville, MD, pp. 224-239, 1977.

[24] Sapareto, S.A., and Dewey, W.C, "Thermal dose determination in cancer therapy," International Journal of Radiation Oncology Biology.Physics, Vol. 10, pp. 787-800, 1984.

[25] Harari, P.M., Hynynen, K.H., Roemer, R.B., Anhalt, D.P., Shimm, D.S., Stea, B., Cassady, J.R., "Development of scanned focussed ultrasound hyperthermia: Clinical response evaluation," International Journal of Radiation Oncology Biology.Physics, Vol. 21, pp. 831-840, 1991.

[26] Shimm, D.S., Hynynen, K.H., Anhalt, D.P., Roemer, R.B., Cassady, J.R., "Scanned focussed ultrasound hyperthermia: Initial clinical results," International Journal of Radiation Oncology Biology.Physics, Vol. 15, pp. 1203-1208, 1988.

[27] Guthkelch, A.N., Carter, L.P., Cassady, J.R., Hynynen, K.H., Iacono, R.P., Johnson, P.C., Obbens, E.A., Roemer, R.B., Seeger, J.F., Shimm, D.S., Stea, B., "Treatment of malignant brain tumors with focused ultrasound hyperthermia and radiation: results of a phase I trial," Journal of Neuro-Oncol., Vol. 10, pp. 271-284, 1991.

[28] Lim, C.M., "Operator user manual for TAU," University of Arizona Cancer Center, Radiation Oncology, 1992.